

---

# DIsoN: Decentralized Isolation Networks for Out-of-Distribution Detection in Medical Imaging

---

Felix Wagner<sup>1</sup>   Pramit Saha<sup>\*1</sup>   Harry Anthony<sup>\*1</sup>  
J. Alison Noble<sup>1</sup>   Konstantinos Kamnitsas<sup>1</sup>

<sup>1</sup>Department of Engineering Science, University of Oxford  
felix.wagner@eng.ox.ac.uk

## Abstract

Safe deployment of machine learning (ML) models in safety-critical domains such as medical imaging requires detecting inputs with characteristics not seen during training, known as out-of-distribution (OOD) detection, to prevent unreliable predictions. Effective OOD detection after deployment could benefit from access to the training data, enabling direct comparison between test samples and the training data distribution to identify differences. State-of-the-art OOD detection methods, however, either discard the training data after deployment or assume that test samples and training data are centrally stored together, an assumption that rarely holds in real-world settings. This is because shipping the training data with the deployed model is usually impossible due to the size of training databases, as well as proprietary or privacy constraints. We introduce the **Isolation Network**, an OOD detection framework that quantifies the difficulty of separating a target test sample from the training data by solving a binary classification task. We then propose **Decentralized Isolation Networks (DIsoN)**, which enables the comparison of training and test data when data-sharing is impossible, by exchanging only model parameters between the remote computational nodes of training and deployment. We further extend DIsoN with class-conditioning, comparing a target sample solely with training data of its predicted class. We evaluate DIsoN on four medical imaging datasets (dermatology, chest X-ray, breast ultrasound, histopathology) across 12 OOD detection tasks. DIsoN performs favorably against existing methods while respecting data-privacy. This decentralized OOD detection framework opens the way for a new type of service that ML developers could provide along with their models: providing remote, secure utilization of their training data for OOD detection services. Code available at: <https://github.com/FelixWag/DIsoN>

## 1 Introduction

Consider the standard setting where an organization, such as a software company, develops and trains a Machine Learning (ML) model to perform a task of interest, for example disease classification in medical images, using a training database. The organization then provides the model to a user (e.g., a client) and deploys it, for example in a hospital, to make predictions on new *test* samples. Because of heterogeneity in real-world data or user-error, a deployed model may receive inputs unlike anything seen in the training data. Such inputs are called out-of-distribution (OOD) samples, in contrast to the in-distribution (ID) samples that follow the distribution of the training data. For example, OOD patterns in medical imaging can be artifacts from suboptimal acquisition or unknown diseases. Performance of ML models often degrades unexpectedly on OOD data [43]. Thus, to ensure safe deployment in safety-critical applications such as healthcare, deployment frameworks should

---

<sup>\*</sup>Equal second-author contribution.

include mechanisms to detect OOD inputs, so that they can be flagged to human users and avoid adverse effects of using potentially wrong model predictions in the downstream workflow.

Multiple OOD detection methods have been previously developed, which can be broadly categorized into *post-hoc* and *training-time regularization* methods [42]. Post-hoc methods assume that a “primary” model has been trained and deployed to perform a task of interest, such as disease classification, and they aim to perform OOD detection without alterations to this primary model [13, 22, 23, 27, 15]. On the other hand, training-time regularization methods alter the embedding space of the primary model during its training, to allow improved OOD detection during inference [30, 29, 5, 14, 36, 28].

Few OOD detection methods leverage direct comparison of test-samples against the training data to identify differences between them for OOD detection, such as KNN-based [34] or density-based methods [6]. These require, however, the training data to be available at the site of deployment, for direct comparison with test-samples. Therefore they are impractical in many applications where sharing and storing the training samples or their embeddings at each site of deployment is impossible due to privacy, legal, or proprietary constraints. Because of this, most other methods do not compare the test-samples against the training data [13, 21] or make indirect comparisons using auxiliary representations of training data, such as via summary statistics [22], prototypes [29, 30] or synthetic samples [7]. Such derived representations, however, do not faithfully capture all intricacies of the original training data. Hypothesizing that direct comparison with the original training data would be useful to infer whether a test sample is OOD, this paper addresses the following question:

*Can we design an OOD detection algorithm that compares test samples against the original training data, without requiring transfer of training data to the point of deployment?*

This paper describes a novel OOD detection framework (Fig. 1) with the following key aspects: (1) We introduce **Isolation Networks** for OOD detection. To infer whether a new test sample is OOD, a neural network is trained to learn a binary classification boundary that separates (isolates) a test sample from the original ID training samples. The network’s convergence rate is then used as a measure of whether the target sample is OOD or similar to the training data. The intuition is that test samples with OOD patterns will be easier to separate from the training samples than ID test samples without OOD patterns. Isolation Networks draw inspiration from Isolation Forests [25], which train decision trees to isolate each training sample. To infer whether a test-sample is OOD, the number of split nodes needed to isolate it is used (c.f. Sec. 2). Isolation Networks instead train a different network for each test sample, to separate it from the training data, and measure convergence as OOD score. (2) We then introduce **Decentralized Isolation Networks (DIsoN)**, a decentralized training framework that enables training Isolation Networks in the practical setting when the ID training data are held on a different computational node than the node of deployment, where the test samples are processed. (3) We extend DIsoN to class-conditional training, where the class of a test sample is first predicted and then used to compare it only against samples in the ID training database of the same class. This reduces variability within the distribution of training samples that the model uses for comparison, making it harder to isolate ID samples that closely resemble their class than OOD samples, improving OOD detection.

We evaluate the capabilities of DIsoN and state-of-the-art OOD detection methods in identifying OOD patterns that occur in real-world applications. For this, we experiment on 4 medical imaging datasets, including dermatology, chest X-rays, breast ultrasound and histopathology, where we

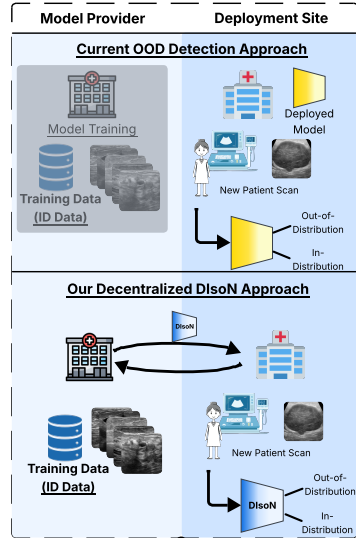


Figure 1: **(Top)** Most OOD detection methods do not use training data after deployment because it cannot be shipped with the model. **(Bottom)** DIsoN enables decentralised comparison of test samples with the training data via model parameter exchange.

evaluate 12 OOD detection tasks. Results show DIsoN outperforms current state-of-the-art methods, demonstrating the effectiveness of remotely obtaining information from the training data during inference to identify unexpected patterns in test samples, while adhering to data-sharing constraints.

## 2 Related Work

**OOD Detection methods.** *Post-hoc methods* for OOD detection assume a "primary" model pre-trained for a task of interest, such as disease classification, and aim to perform OOD detection without modifying it. A common baseline is using Maximum Softmax Probability (MSP) [13] as a measure of whether a test sample is OOD. Another common approach is to represent the training data via summary statistics, such as using class-conditional Gaussians in the model’s latent space, and use Mahalanobis distance to detect OOD samples [13]. In a similar fashion, other post-hoc approaches use the logit space (energy score [27]), gradient space, (GradNorm [15]) and feature space (fDBD [26]), or combine multiple representations (ViM [37]) to derive a measure for OOD detection. Another group of methods use *training-time regularization*. Regularization modifies the embedding space of the primary model during training to bolster OOD detection performance at inference [14, 5, 39, 9]. A representative example of the state-of-the-art is CIDER [30], which uses a loss function to optimize the model’s feature space for intra-class compactness and inter-class dispersion. Recently, PALM [29] this further by modeling each class with multiple prototypes.

Most OOD detection methods, such as the above, do not directly utilize the training data after the model’s deployment. Thus they do not directly compare them with the test samples processed after deployment, which could facilitate detecting patterns that differentiate them. There are few notable exceptions, such methods based on KNN [34] and Local Outlier Factor [6]. These compare an input’s embedding to the training data embeddings. They require, however, shipping and storing the training data or their feature vectors to each deployment site, which in many practical applications can be infeasible due to privacy constraints or the size of training databases.

Inspiration for this work was drawn from the seminal work on Isolation Forests (iForest [25]), which has received multiple extensions such as Deep Isolation Forests [40]. They train decision trees using the original ID training data or their deep embeddings respectively, to learn partitions that isolate each sample. To infer whether a test-sample is OOD, they count the number of split nodes applied by the trained trees until it is isolated. OOD samples should need less splits than ID nodes. The algorithm introduced herein trains a neural network classifier to isolate a single test-sample from the ID training data, focusing on extracting patterns that distinguish the specific sample. We demonstrate the use of convergence rate as scoring function to infer whether a test-sample is OOD. We also demonstrate the use of decentralised training to enable such an isolation algorithm without data-sharing.

**Federated Learning and OOD Detection.** Training of DIsoN uses decentralised optimization similar to Federated Learning (FL). Using FL for OOD detection is a recent area. The few related works, such as [44, 24], studied settings significantly different from ours: they assume the training data is decentralized across multiple computational nodes, where each node’s data follow a different distribution. Using FL, they train a model that measures distribution-shifts between nodes. After training, the model is applied on test-samples for OOD detection. Our algorithm does not require training data from multiple distributions or multiple nodes. It assumes one node holds all ID training data and a second node holds a single test-sample, which we infer whether it is OOD via decentralised training of a binary classifier. Thus the motivation, use-case and technical challenges are distinct. Moreover, DIsoN may resemble FL with a few-shot client [33, 38]. Few-shot methods are designed to regularize against overfitting the limited data of few-shot client(s), to train a model for a predictive task (e.g. disease diagnosis) that generalizes to new samples. DIsoN does not train a model for generalization. It optimizes for distinguishing data of the source node from a target sample, using convergence speed to infer if the latter is OOD. Hence, few-shot methods are not directly applicable.

## 3 Method

**Preliminary: Out-of-Distribution Detection.** Let  $\mathcal{X}$  be the input data space and  $\mathcal{Y} = \{1, 2, \dots, C\}$  the label space for a classification task with  $C$  classes. We denote the *source training dataset* as  $\mathcal{D}_s = \{(\mathbf{x}_i, y_i)\}_{i=1}^N$ , assumed *i.i.d.* from the joint distribution  $\mathbb{P}_{\mathcal{X}\mathcal{Y}}$ . The marginal distribution over the input data space  $\mathcal{X}$  is denoted as  $\mathbb{P}_{\mathcal{X}}^{in}$ . The goal of OOD detection is to determine, during

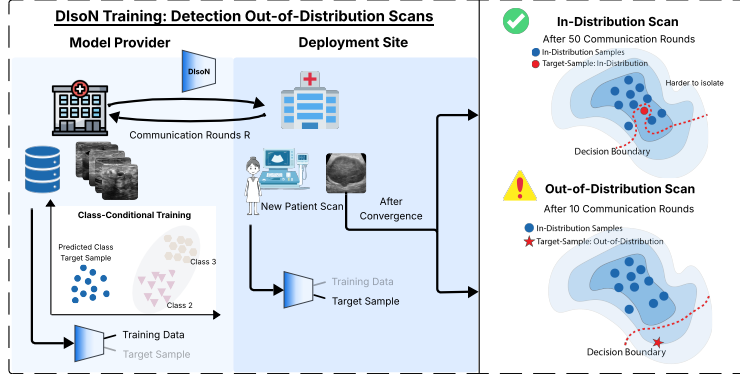


Figure 2: **Overview of DiSoN:** When a new scan is obtained at the deployment site, DiSoN is trained using parameter updates from both the deployment site and the model provider, who holds the ID training data, to isolate the target sample from the training data. The deployment site trains on the single target scan, while the model provider trains on the source data (optionally class-conditioned). Only model parameters are exchanged. **(Right)** After convergence, the scan is classified as OOD if it is isolated in few rounds, and as ID otherwise.

inference, whether a *target sample*  $\mathbf{x}_t \in \mathcal{X}$  originates from the source distribution  $\mathbb{P}_{\mathcal{X}}^{in}$ , or an unknown OOD distribution  $\mathbb{P}_{\mathcal{X}}^{out}$ . This can be achieved by defining an OOD scoring function  $S : \mathcal{X} \rightarrow \mathbb{R}$ , that assigns high scores to ID samples and low scores to OOD samples. We label a sample  $\mathbf{x}$  as OOD when the scoring function  $S(\mathbf{x}) < s^*$ , and ID if  $S(\mathbf{x}) \geq s^*$ , with a chosen threshold  $s^*$ .

### 3.1 Isolation Networks

The core idea of our approach is that the difficulty of training a binary classifier to separate a single target sample  $\mathbf{x}_t$  from the source data  $\mathcal{D}_s$  gives an indication whether  $\mathbf{x}_t$  is ID or OOD. Intuitively, a target sample that is ID will share characteristics with samples in  $\mathcal{D}_s$ . As a result, it is *harder* for a classifier to isolate (separate) the target sample and will require more update steps. On the other hand, an OOD target sample has patterns that differ from  $\mathcal{D}_s$ , making it *easier* to isolate and requiring fewer update steps during training. Fig. 2 gives a visual intuition of the idea.

Formally, we consider a neural network consisting of a feature extractor  $f : \mathcal{X} \rightarrow \mathcal{Z}$ , parameterized by  $\theta^f$ , and a binary classification head  $h : \mathcal{Z} \rightarrow [0, 1]$ , with parameters  $\theta^h$ . The full network is parameterized by  $\theta = (\theta^f, \theta^h)$ . We use  $m \in \{0, 1\}$  for isolation labels and reserve  $y$  for class labels. In an *idealized* centralized setting with full access to  $\mathcal{D}_s$  and the target sample  $\mathbf{x}_t$ , we can train the network  $h \circ f$  for the following binary classification problem: Assign label  $m = 0$  to all source samples  $\mathbf{x}_s \in \mathcal{D}_s$  and label  $m = 1$  to the target sample  $\mathbf{x}_t$ . Typically,  $\mathcal{D}_s$  has a high number of samples compared to the single target sample  $\mathbf{x}_t$ ,  $|\mathcal{D}_s| \gg 1$ . Therefore, directly training on this highly imbalanced setup is suboptimal, as it can lead to a trivial classifier that always predicts the majority class ( $m = 0$ ), ignoring the minority class ( $m = 1$ ). To ensure that the target sample has an impact during training, we *over-sample*  $\mathbf{x}_t$  within each mini-batch. Specifically, we construct mini-batches as  $B = B_s \cup \{\mathbf{x}_t^{(1)}, \dots, \mathbf{x}_t^{(N)}\}$ , where  $B_s$  is a set of source samples drawn from  $\mathcal{D}_s$ , and  $\{\mathbf{x}_t^{(1)}, \dots, \mathbf{x}_t^{(N)}\}$  are  $N$  replicated copies of the same target sample  $\mathbf{x}_t$ . The empirical loss for this optimization objective is:

$$\mathcal{L}_c(\theta; B_s, \mathbf{x}_t, N) = \frac{1}{|B_s| + N} \left( \sum_{\mathbf{x}_s \in B_s} L(\theta; \mathbf{x}_s, m = 0) + N \cdot L(\theta; \mathbf{x}_t, m = 1) \right), \quad (1)$$

where  $L(\theta; x, m)$  denotes the binary cross-entropy loss. In Sec. 3.2 we compare the gradient of the centralized version  $g_c(\theta; B_s, \mathbf{x}_t, N) = \nabla_{\theta} \mathcal{L}_c(\theta; B_s, \mathbf{x}_t, N)$  to our proposed decentralized version.

**Convergence Time as OOD Score.** To quantify the “isolation difficulty”, we track the number of training steps required by the binary classifier to separate  $\mathbf{x}_t$  from  $\mathcal{D}_s$ . Let  $\theta^{(k)}$  be the model parameters after  $k$  optimization steps with a stochastic gradient-based optimizer (e.g. SGD or Adam [20]) using the gradients from the loss of Eq.1. Formally, we define our convergence time  $K$  as:

**Definition 3.1** (Convergence Time  $K$ ). Let  $p^{(k)}(x) = h(f(x; \theta^{(k)}))$  be the sigmoid-score after  $k$  updates. Fix a window  $E_{\text{stab}} \in \mathbb{N}$  and accuracy threshold  $\tau \in (0, 1]$ . The convergence time  $K$  is the smallest  $k \geq E_{\text{stab}}$  such that

$$\min_{j \in [k - E_{\text{stab}} + 1, k]} p^{(j)}(x_t) > 0.5 \quad \text{and} \quad \frac{1}{|\mathcal{D}_s|} \sum_{x_s \in \mathcal{D}_s} \mathbb{I}\{p^{(k)}(x_s) \leq 0.5\} \geq \tau.$$

Intuitively, the conditions ensure that the classifier correctly classifies  $\mathbf{x}_t$  for the last  $E_{\text{stab}}$  consecutive updates (first condition), while achieving an accuracy of at least  $\tau$  on the source data (second condition). We set  $E_{\text{stab}} = 5$  and  $\tau = 0.85$ . Further details on these parameter choices are provided in the Appendix D. We define our OOD scoring function as  $S(\mathbf{x}_t) = K$ , following the convention where ID samples have higher scores. We emphasize that this setup corresponds to the centralized version of the algorithm, where both  $D_s$  and  $x_t$  are accessible on the same node. In Sec. 3.2, we extend it to the decentralized case, where source data and the target sample reside on separate nodes.

### 3.2 Decentralized Isolation Networks (DIsoN)

**Problem Setting: Decentralized OOD Detection.** The Isolation Network described above assumes direct access to both the source data  $\mathcal{D}_s$  and the target sample  $\mathbf{x}_t$ . However, as described in Sec.1, this assumption does not hold in many real-world settings. We therefore formalize a decentralized setting involving two sites: the *Source Node* (SN) and the *Target Node* (TN). SN represents a model provider that holds the source training dataset  $\mathcal{D}_s$ , on which it has pre-trained a primary model  $M_{pre}$  for the main task of interest, such as a  $C$ -class classifier of disease.  $M_{pre}$  consists of a feature extractor (parameterized by  $\theta^{pre}$ ) and a  $C$ -class classification head. TN holds target samples  $\mathbf{x}_t$  and represents the site where  $M_{pre}$  is deployed to process  $\mathbf{x}_t$ . Therefore, the aim of the OOD detection algorithm is to infer whether a given  $\mathbf{x}_t$  on TN is ID or OOD, to support safe operation of  $M_{pre}$ . To this end, TN can exchange model parameters with SN, but not raw data or their embeddings due to privacy and regulatory constraints.

**DIsoN Method Overview.** To approximate the training dynamics of an Isolation Network (Sec. 3.1) without data sharing and without requiring centralized access to both the source data and target samples, we propose DIsoN. Fig.2 shows an overview of DIsoN. Inspired by the Federated Learning framework, our algorithm trains parameters of an Isolation Network over multiple communications rounds between SN and TN. We keep track of a *global* set of Isolation Network parameters. At the start of each round  $r$ , they are transmitted to SN and TN. In each round  $r$ , both SN and TN update them locally by performing  $E \geq 1$  local optimization steps. At the end of a round, the global set of parameters is updated via a weighted aggregation of the local updates. In more detail:

**1) Initialization.** Let  $\theta^{(r)}$  be the global model parameters of the Isolation Network at the start of round  $r$ . The feature extractor  $\theta^f$  of the initial global model  $\theta^{(0)} = (\theta^f, \theta^h)$  is initialized with the pre-trained parameters  $\theta^{pre}$  of primary model  $M_{pre}$ , while the binary classification head is initialized randomly. This initialization is done on SN, after which  $\theta^{(0)}$  is transmitted to TN.

**2) Local Updates.** Each site performs local training for  $E$  steps using its own data: The **Source Node** initializes its local model  $\theta_S^{(r,0)} = \theta^{(r)}$  and performs  $E$  optimization steps on mini-batches  $B_s \sim \mathcal{D}_s$ , minimizing  $L(\theta; \mathbf{x}_s, 0)$ , resulting in  $\theta_S^{(r,E)}$ . Similarly, the **Target Node** initializes its local model  $\theta_T^{(r,0)} = \theta^{(r)}$  and performs  $E$  optimization steps on the single target sample  $\mathbf{x}_t$ , minimizing  $L(\theta; \mathbf{x}_t, 1)$ , resulting in  $\theta_T^{(r,E)}$ .

**3) Model Aggregation.** After local updates, TN sends  $\theta_T^{(r,E)}$  back to SN. The models are then aggregated into an updated global model using weighted averaging:

$$\theta^{(r+1)} = \alpha \cdot \theta_S^{(r,E)} + \beta \cdot \theta_T^{(r,E)}, \quad (2)$$

where the aggregation weights are  $\beta = 1 - \alpha$ . The updated global model  $\theta^{(r+1)}$  is then sent to TN to start the next local training round.

Before each local training round starts, we evaluate the current global model  $\theta^{(r)}$  using the convergence criteria in Def. 3.1 (TN evaluates on  $\mathbf{x}_t$ , SN on  $\mathcal{D}_s$ ). If converged, we record  $R = r$  and terminate. The OOD score for the target sample  $\mathbf{x}_t$  in the decentralized setting is based on the

number of communication rounds  $R$  required to converge, analogous to the number of steps  $K$  in the centralized case:  $S_{\text{DIsoN}}(\mathbf{x}_t) = R$ . We can draw a connection between DIsoN and our centralized version. We show that under specific conditions, the decentralized and the centralized versions result in equivalent model parameters:

**Proposition 3.1** (DIsoN and Centralized Isolation Network Equivalence for  $E = 1$ ). *Let  $\theta_{\text{cent}}$  be the model parameters from our centralized algorithm and  $\theta_{\text{dec}}$  be the parameters from DIsoN. Let each site perform one local SGD step ( $E = 1$ ) with learning rate  $\eta$ , and aggregate with  $\alpha = \frac{|B_s|}{|B_s|+N}$ ,  $\beta = \frac{N}{|B_s|+N}$ . Then the decentralized update equals the centralized one:*

$$\theta_{\text{dec}}^{(r+1)} = \theta^{(r)} - \eta(\alpha g_S(\theta^{(r)}) + \beta g_T(\theta^{(r)})) = \theta^{(r)} - \eta g_c(\theta^{(r)}) = \theta_{\text{cent}}^{(r+1)},$$

where  $g_S(\theta) = \frac{1}{|B_s|} \sum_{\mathbf{x}_s \in B_s} \nabla_{\theta} L(\theta; \mathbf{x}_s, 0)$ ,  $g_T(\theta) = \nabla_{\theta} L(\theta; \mathbf{x}_t, 1)$  and  $N$  is the number of times  $\mathbf{x}_t$  is oversampled in the centralized version.

*Proof sketch.* Insert  $\theta_S^{(r,1)} = \theta^{(r)} - \eta g_S(\theta^{(r)})$ ,  $\theta_T^{(r,1)} = \theta^{(r)} - \eta g_T(\theta^{(r)})$  into the weighted average; factor out  $\theta^{(r)}$ , use  $\beta = 1 - \alpha$ . Full derivation can be found in the Appendix.  $\square$

Prop. 3.1 shows that our decentralized training exactly replicates the centralized version when  $E = 1$  and aggregation weights are chosen accordingly. This theoretical equivalence motivated our design of DIsoN: it preserves the core idea of the Isolation Network, while meeting our decentralized data sharing constraints. In practice, we allow  $E > 1$  to reduce communication overhead, which causes the decentralized updates to deviate from the centralized version. However, as we show in Sec. 4, DIsoN achieves promising results even with the approximation. We found DIsoN to be robust across a broad range of  $\alpha$  values, as shown in an ablation study in Sec. 4.2.

**Practical Techniques: Augmentation and Normalization.** One challenge in DIsoN is to avoid rapid memorization and overfitting of superficial features in the target sample  $\mathbf{x}_t$ , making the isolation task trivial regardless whether the sample is OOD. To prevent this, we apply stochastic data augmentations (e.g. random crops, horizontal flips), which regularize the model to learn invariant features, so that the separation is based on semantic characteristics. Furthermore, in DIsoN, we use Instance Normalization (IN) [35] instead of the widely used Batch Normalization (BN) [16] layers for feature normalization. BN relies on batch-level statistics, which are not suitable for our single-sample TN. IN instead normalizes each feature map per sample and therefore fits better for our decentralized, single target sample scenario.

### 3.3 Class-Conditional Decentralized Isolation Networks (CC-DIsoN)

To further improve DIsoN, we introduce its class-conditional variant, **CC-DIsoN**. The intuition is that ID samples should be especially hard to isolate from source samples of the same class, as they are likely to share similar visual features compared to samples from other classes. To use this idea, we modify the source data sampling strategy during local training at SN. After the initialization phase, TN uses the pre-trained model  $M_{\text{pre}}$  to predict the class of the target sample:  $\hat{y} = \arg \max_c [M_{\text{pre}}(\mathbf{x}_t)]_c$ . Afterwards, TN sends the predicted label  $\hat{y}$  to SN. During local training at SN, mini-batches are now sampled *only* from source data from class  $\hat{y}$ :  $B_s \subset \{(\mathbf{x}_s, y_s) \in \mathcal{D}_s \mid y_s = \hat{y}\}$ . The other steps of our method remain the same. Our empirical results in Sec. 4.2 confirm that this improves OOD detection.

## 4 Experiments & Results

**Datasets.** We evaluate DIsoN on four publicly available medical imaging benchmark datasets covering dermatology, breast ultrasound, chest X-ray, and histopathology. All datasets consist of real, clinically acquired images and no synthetic data is used. The first three benchmarks use images with naturally occurring non-diagnostic artifacts as OOD samples (e.g., rulers, pacemakers, annotations), while histopathology focuses on semantic and covariate shifts across domains. Example images are shown in Fig.3.

**Dermatology & Breast Ultrasound:** We adopt the benchmark setup from [3], using images without artifacts as the training and ID test data, and images with artifacts (rulers and annotations) as OOD samples. For breast ultrasound (BreastMNIST [41]), the artefacts are embedded text annotations, and

for dermatology (D7P [19]) the artefacts are black overlaid rulers. For breast ultrasound, the primary model  $M_{pre}$  is trained for 3-class classification (normal/benign/malignant). The 228 annotated scans with artifacts are used as OOD test samples, while the remaining artifact-free scans are split 90/10 into training and ID test sets. For dermatology, the primary model  $M_{pre}$  is trained for binary classification (nevus/non-nevus). The annotated 251 images with rulers are used as OOD samples and the remaining 1403 are split 90/10. Images are resized to  $224 \times 224$ .

**Chest X-Ray:** Following the benchmark from [2], we use frontal-view X-ray scans (from CheXpert [17]) containing no-support devices as the training and ID test data, and scans containing pacemakers as OOD samples. The primary model  $M_{pre}$  was trained for the binary classification of cardiomegaly. We use the 23,345 annotated scans without any support devices as our training data, and randomly hold out 1000 ID samples for testing. The OOD test set includes 1000 randomly sampled scans with pacemakers. All images are resized to  $224 \times 224$ .

**Histopathology:** We use the MIDOG benchmark from OpenMIBOOD [11]. The MIDOG dataset [4] consists of  $50 \times 50$  image patches extracted from Hematoxylin & Eosin-stained histological whole-slide images, grouped into different "domain" data sets corresponding to different imaging hardware, staining protocols, or cancer types. The primary model is trained for 3-class classification (mitotic/imposter/other) on domain 1a. Following [4] we evaluate on two settings: (i) **Near-OOD:** Domains 2-7 are treated as separate OOD detection task with only moderate domain shifts. (ii) **Far-OOD:** Using CCAgT [1] and FNAC 2019 [32] dataset as the OOD task, which differ significantly due to being completely different medical applications. We use the 251 test ID samples from domain 1a and randomly sample 500 OOD samples from each of the near- and far-OOD domains.

**Training Details.** We use a ResNet18 [12] with Instance Normalization (as per Sec.3.2) pre-trained on the dataset-specific task as initialization for DIsoN. DIsoN is trained with Adam (lr=0.001 for dermatology and ultrasound; 0.003 for X-ray). For histopathology SGD with momentum (lr=0.01, momentum=0.9) is used (since [11] suggests pretraining with SGD). Local iterations per communication round are chosen to approximately match one epoch on the training data. We use standard augmentations (e.g. random cropping, rotation, color-jitter) and the aggregation weight is fixed to  $\alpha = 0.8$ , since it performs consistently well across all our experiments (see Sec. 4.2 for effect of  $\alpha$ ). Experiments were run on an NVIDIA RTX A5000. More training details and hyperparameters are provided in the Appendix. OOD detection performance is evaluated with two metrics: (i) area under the receiver operating characteristics curve (AUROC, higher is better) (ii) the false positive rate at 95% true positive rate (FPR95, lower is better). All results in Tables 1 and 2 are averaged over three runs with different seeds, and we report mean and standard deviation. Standard deviations for Tab.2 are in Appendix I due to space limitations.

**Baselines.** We compare our method against state-of-the-art OOD detection methods from the two main categories: *post-hoc* and *training-time regularization* methods. The post-hoc methods include: MSP [13], MDS [22], fDBD [26], ViM [37], Deep iForest [40]. For *training-time regularization methods*, we evaluate the recent methods CIDER [30] and PALM [29] (both using contrastive learning). We use MDS for OOD scoring on their learned feature representations. Several baselines already use a form of class-conditioning based on the model’s predicted class: MDS, PALM, and CIDER via Mahalanobis distances to class clusters; ViM uses the maximum logit of the predicted class; MSP via softmax probability; and fDBD via distance to the decision boundary (all implicitly or explicitly conditioned on the predicted class). Only iForest does not. CC-DIsoN similarly relies solely on the predicted class from  $M_{pre}$  for class-conditional sampling and uses no ground-truth labels, providing no additional information beyond these methods.

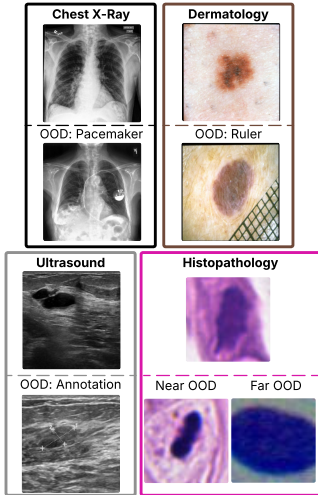


Figure 3: **Examples of data.** **X-Ray:** ID X-ray vs. OOD scan with pacemaker. **Dermatology:** ID lesion vs. OOD image with ruler. **Ultrasound:** ID artifact-free ultrasound vs. OOD scan containing annotations. **Histopathology:** ID mitotic-cell patch vs. near-OOD patch with different cancer type and far-OOD patch with different staining.

Table 1: OOD detection performance evaluated on three OOD datasets: Chest X-Ray, Dermatology, and Breast Ultrasound and reported as mean  $\pm$  standard deviation over three random seeds.  $\downarrow$  means smaller is better and  $\uparrow$  means larger is better. **Bold** numbers highlight the best results, second best results are underlined.

Method	Chest X-Ray		Dermatology		Breast Ultrasound		Average	
	AUROC $\uparrow$	FPR95 $\downarrow$						
MSP	60.44 $\pm$ 4.2	100.00 $\pm$ 0.0	65.39 $\pm$ 3.9	100.00 $\pm$ 0.0	58.85 $\pm$ 4.5	100.00 $\pm$ 0.0	61.56 $\pm$ 2.0	100.00 $\pm$ 0.0
MDS	53.82 $\pm$ 1.5	90.47 $\pm$ 1.0	69.36 $\pm$ 5.5	76.06 $\pm$ 15.5	<u>61.02<math>\pm</math>1.7</u>	<u>74.40<math>\pm</math>1.0</u>	61.40 $\pm$ 2.5	80.31 $\pm$ 5.5
fDBD	68.26 $\pm$ 0.4	<u>78.07<math>\pm</math>5.4</u>	63.59 $\pm$ 2.5	88.26 $\pm$ 10.8	60.73 $\pm$ 2.1	87.50 $\pm$ 4.7	64.19 $\pm$ 1.6	84.61 $\pm$ 5.5
ViM	62.60 $\pm$ 4.8	85.80 $\pm$ 7.3	68.39 $\pm$ 2.0	75.35 $\pm$ 6.1	59.44 $\pm$ 2.8	<b>73.21<math>\pm</math>3.1</b>	63.48 $\pm$ 1.5	78.12 $\pm$ 4.2
iForest	56.35 $\pm$ 5.6	88.27 $\pm$ 5.1	56.68 $\pm$ 6.8	87.31 $\pm$ 3.7	47.02 $\pm$ 4.8	95.82 $\pm$ 2.1	53.35 $\pm$ 3.3	90.47 $\pm$ 1.5
CIDER	<u>70.47<math>\pm</math>6.3</u>	79.00 $\pm$ 9.9	<u>81.98<math>\pm</math>2.8</u>	56.57 $\pm$ 8.2	58.03 $\pm$ 3.1	82.73 $\pm$ 5.2	<u>70.16<math>\pm</math>3.4</u>	<u>72.77<math>\pm</math>2.5</u>
PALM	65.41 $\pm$ 6.5	85.73 $\pm$ 9.2	77.25 $\pm$ 1.0	62.44 $\pm$ 0.8	59.35 $\pm$ 3.1	75.60 $\pm$ 5.5	67.34 $\pm$ 1.4	74.59 $\pm$ 1.9
<b>CC-DIsoN</b>	<b>84.94<math>\pm</math>0.9</b>	<b>61.85<math>\pm</math>1.2</b>	<b>89.54<math>\pm</math>1.5</b>	<b>42.49<math>\pm</math>4.4</b>	<b>65.62<math>\pm</math>1.2</b>	<b>73.21<math>\pm</math>4.7</b>	<b>80.00<math>\pm</math>0.7</b>	<b>59.20<math>\pm</math>3.1</b>

Table 2: OOD detection performance across nine different OOD detection task of MIDOG, split into near-OOD and far-OOD setting. Each cell shows AUROC $\uparrow$ /FPR95 $\downarrow$ , reported as mean over three random seeds. **Bold** numbers highlight the best results, second best results are underlined.

Methods	near-OOD								far-OOD		
	2	3	4	5	6a	6b	7	Avg.	CCAgT	FNAC	Avg.
MSP	54.1/94.8	47.4/93.4	55.7/89.4	59.0/93.5	54.8/94.7	45.6/95.5	56.1/92.4	53.3/93.4	78.4/52.2	82.7/63.6	80.6/57.9
MDS	67.4/80.0	<u>67.2/79.8</u>	65.7/81.9	61.2/87.4	60.6/87.4	55.5/89.5	51.0/91.6	61.2/85.4	87.1/43.6	86.6/39.6	86.8/41.6
fDBD	57.9/83.0	52.5/81.4	57.5/88.7	60.2/89.0	57.9/85.9	51.2/86.2	55.2/92.2	56.1/86.6	74.6/58.3	82.1/63.7	78.3/61.0
ViM	68.0/79.8	66.7/ <u>77.8</u>	66.2/ <u>77.7</u>	63.5/ <b>86.9</b>	61.9/87.3	55.7/91.0	54.9/93.1	<u>62.4/84.8</u>	92.5/29.1	<u>92.6/27.0</u>	92.6/28.0
iForest	37.9/98.3	38.6/96.9	39.7/97.7	41.6/97.5	39.5/98.0	40.4/97.7	46.4/95.7	40.6/97.4	27.7/99.2	32.3/96.8	30.0/98.0
CIDER	71.4/84.6	65.6/89.0	55.5/91.5	<u>64.2/89.8</u>	57.4/92.2	47.7/96.5	<b>64.1/88.2</b>	60.9/90.2	82.5/77.2	95.4/18.3	89.0/47.8
PALM	<u>73.5/78.1</u>	59.2/90.3	<u>66.3/77.7</u>	<b>64.3/93.6</b>	62.1/90.8	41.8/97.6	61.6/93.6	61.2/88.8	<u>97.0/21.8</u>	<b>99.6/1.5</b>	<b>98.3/11.6</b>
<b>CC-DIsoN</b>	<b>75.4/78.8</b>	<b>79.5/61.7</b>	<u>72.6/79.7</u>	63.0/89.4	<b>64.0/85.3</b>	<b>70.7/79.9</b>	<u>61.8/92.0</u>	<b>69.6/81.0</b>	<b>98.3/4.8</b>	<u>98.4/4.0</u>	<b>98.3/4.4</b>

#### 4.1 Evaluation on Medical OOD Benchmarks

**Dermatology, Chest X-Ray and Breast Ultrasound.** Tab. 1 compares CC-DIsoN with the baselines on our three medical OOD benchmarks where the OOD task is to detect artifacts. We can see that the post-hoc methods struggle to detect these domain-specific artifacts: fDBD and ViM average only between 63 – 64% AUROC while having a high FPR95 (84.6% and 78.1%, respectively). Training-time regularization methods like CIDER do better (70.2% average AUROC), but still have a high FPR95 of 72.8%. CC-DIsoN performs strongly compared to the baselines and shows consistent improvement across all datasets. Compared to fDBD, it improves AUROC by **15.8%** and reduces FPR95 by **25.4%**. Against the best baseline (CIDER), it improves AUROC by **9.8%** and lowers FPR95 by **13.6%**. This demonstrates that directly comparing test samples against the training data during inference has a positive impact on OOD detection.

**Effects of Class-Conditioning.** Tab. 3a shows the benefits of class-conditioning (Sec. 3.3). On average, CC-DIsoN improves AUROC by 1.7%. More notably, CC-DIsoN reduces FPR95 by **8.2%** across all three datasets. Class-conditioning consistently lowers FPR95, demonstrating that focusing the isolation task on the predicted same-class samples improves OOD detection.

Table 3: (a) Comparison of DIsoN and CC-DIsoN on three medical datasets using AUROC (higher is better) and FPR95 (lower is better). (b) Effect of incorrect predicted classes for class-conditional sampling in CC-DIsoN (AUROC). “Best Baseline” is the strongest baseline from Tab. 1 (for reference); “ID & OOD wrong”: all targets assigned incorrect classes; “ID wrong”: only ID targets assigned incorrect classes; “OOD wrong”: only OOD targets assigned incorrect classes.

(a)					(b)					
Dataset	AUROC $\uparrow$		FPR95 $\downarrow$		Dataset	Best Baseline	Standard CC-DIsoN	ID & OOD wrong	ID wrong	OOD wrong
	DIsoN	CC-DIsoN	DIsoN	CC-DIsoN						
Ultrasound	<b>67.0</b>	65.6	78.6	<b>73.2</b>	Ultrasound	61.0	65.6	61.5	34.6	89.6
Dermatology	86.4	<b>89.5</b>	50.0	<b>42.5</b>	Dermatology	82.0	89.5	83.1	84.7	86.7
X-Ray	81.4	<b>84.9</b>	73.6	<b>61.9</b>	X-Ray	70.5	84.9	77.9	74.0	88.3
<b>Average</b>	78.3	<b>80.0</b>	67.4	<b>59.2</b>						

**Impact of Predicted Class Accuracy.** Since CC-DIsoN conditions on the predicted class from the pre-trained model  $M_{pre}$ , we analyse how misclassification affect its performance. We simulate three

controlled scenarios by assigning wrong predicted classes to: (i) all target samples (ID & OOD), (ii) only ID targets while OOD targets use their predicted classes, and (iii) only OOD targets while ID targets use their predicted classes. Results in Tab.3b show that performance drops mainly when ID targets are incorrect, as class-conditioning compares them to unrelated classes, making isolation easier and reducing the separation in convergence rounds between ID and OOD samples. In contrast, performance slightly increases when OOD targets are mislabeled, as comparing them to unrelated classes makes convergence faster. Even under such extreme settings, CC-DIsoN remains competitive. Further details are provided in the Appendix E.

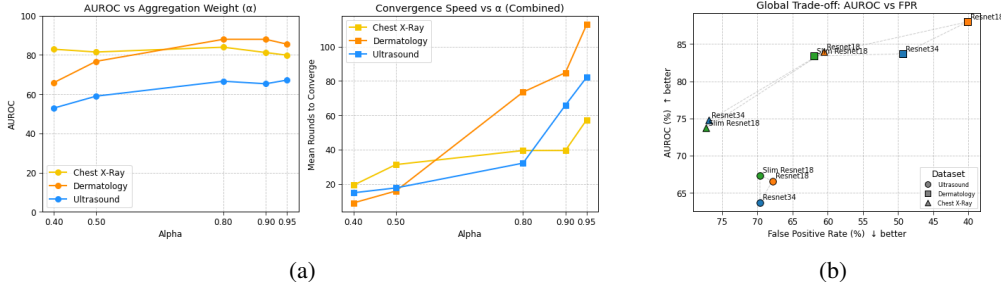


Figure 4: **(a) Effect of aggregation weight  $\alpha$ .** Left: AUROC vs.  $\alpha$ . Higher  $\alpha$  improves OOD detection by emphasizing the source updates. Right: Mean number of communication rounds until convergence (ID and OOD targets combined). Trade-off: Lower  $\alpha$  values speed up convergence but reduce OOD performance. **(b) Network Size.** Global AUROC vs. FPR95 plot for three backbones (Slim ResNet18, ResNet18, ResNet34) across the same datasets. ResNet18 gives the balance between AUROC and FPR95. Grey dashed lines link backbones per dataset.

**Histopathology: MIDOG.** While earlier benchmarks focused on detecting non-diagnostic artifacts as OOD task, MIDOG evaluates semantic and covariate shift as OOD task. Tab. 2 shows that CC-DIsoN also performs strongly in this setting. In the most challenging near-OOD setting, CC-DIsoN achieves an average AUROC of 69.6%, which is a **8.4%** improvement compared to the best regularization-based method PALM and a **7.2%** gain compared to the best post-hoc method ViM. It also achieves the lowest FPR95 in this setting, albeit with a smaller margin. In the less challenging far-OOD setting, CC-DIsoN achieves an AUROC of 98.3% and a FPR95 of 4.4%, indicating almost perfect separation. Out of all compared methods, only PALM achieves same AUROC performance in the far-OOD task, although CC-DIsoN performs better in the near-OOD task. IForests were originally developed for tabular data, where they perform well. However, prior works [34, 10] shows poor performance on high-dimensional imaging data, which explains the low AUROC in our experiments. Overall, these results demonstrate that CC-DIsoN does not only perform well for OOD tasks with localised artifacts but also effective in identifying semantic and covariate shifts across medical imaging tasks.

## 4.2 Further Analysis of DIsoN

**Sensitivity Analysis of Hyperparameter  $\alpha$ .** We analyze the effect of the aggregation weight  $\alpha$  (Eq. 2) on both the OOD detection performance and convergence rate across Dermatology, Ultrasound, and X-Ray in Fig. 4a. We can see that lower  $\alpha$  values, which give relatively more weight to the target updates, reduce OOD detection performance, since the isolation task becomes dominated by the target sample, and loses the comparison signal to the source data. Increasing  $\alpha$  improves AUROC consistently across datasets, with performance plateauing at  $\alpha = 0.8$ . This shows that a stronger emphasis on training data improves the isolation-based OOD performance. However, the number of communication rounds required for convergence increases with  $\alpha$ . This aligns with Proposition 3.1, where  $\alpha$  controls the implicit oversampling ratio  $N$ : smaller  $\alpha$  increases the target signal (larger  $N$ ) (faster isolation), while larger  $\alpha$  slows convergence (more rounds needed to incorporate the target’s signal). In practice, this creates a trade-off between convergence speed and detection performance. The goal of this analysis is not to identify one “optimal” value of  $\alpha$ , but to show that our method remains robust across a wide range of values. Performance stays quiet stable for  $\alpha$  between 0.5 and 0.95 (Fig. 4a), suggesting good generalization across tasks without extensive hyperparameter tuning.

**Effect of Network Size.** To quantify how capacity of the Isolation Network affects the OOD scores, we compare three network sizes: a “Slim” ResNet18 (0.5 $\times$  channel widths), the standard

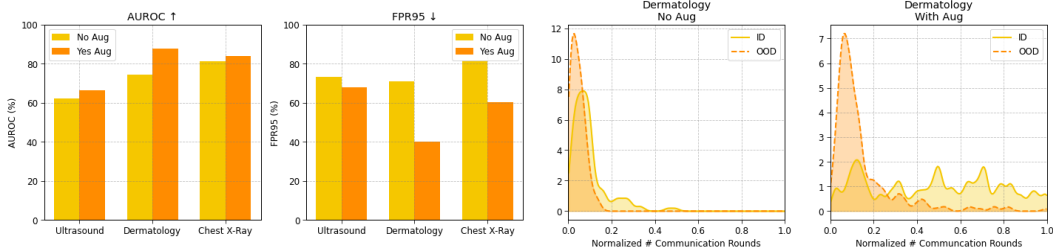


Figure 5: **Effect of image augmentation.** Left: Bar plots show that using random augmentation (“Yes Aug”) during training improves AUROC and FPR95 for three datasets. Right: Density plots for dermatology: without augmentation, ID and OOD curves overlap heavily, whereas with augmentation OOD samples isolate fast and ID samples require more updates.

ResNet18, and a deeper ResNet34. Fig. 4b shows each backbone’s AUROC vs. FPR95 trade-off on Breast Ultrasound (circles), Dermatology (squares), and Chest X-Ray (triangles). Neither the Slim-ResNet18 nor the ResNet34 outperforms the standard ResNet18: the slim model might lack sufficient representational capacity to detect the subtle visual difference, while the deeper network does not yield consistent OOD gains and roughly doubling the required compute. This is likely because a binary isolation task does not require this excessive parameter capacity. Therefore, ResNet18 gives the best balance between good ID/OOD separation and computational efficiency.

**Effect of Image Augmentations.** Fig. 5 shows the effects of applying image augmentations during DIsoN training on Ultrasound, Dermatology, and X-Ray. Augmentations consistently improves AUROC: **+4.43%** on Ultrasound, **+13.69%** on Dermatology, and **+2.76%** on X-ray. FPR95 also decreases, most notably on Dermatology **-30.99%**. The density plot of dermatology dataset shows that without augmentation, ID and OOD samples converge in similar number of few rounds, resulting in poor separation. With augmentations, OOD target samples isolate quickly, but ID target samples require many more rounds. This demonstrates the regularization effect of augmentations: they prevent the model from quickly memorizing a single target sample, regardless of whether it is ID or OOD.

**Runtime Analysis and Practical Considerations.** We extend the runtime analysis in Fig. 4a by reporting detailed statistics, including quantiles and results across different  $\alpha$  values, in Appendix G. Since wall-clock time depends on hardware and network conditions, we primarily measure runtime in communication rounds, offering a hardware-independent estimate. Although DIsoN introduces extra computation, as each target sample requires an isolation task, this design trades speed for improved OOD detection performance. In practice, real-time inference is rarely required in healthcare, where scans are often reviewed hours or days later [31] (except in emergencies), and diagnostic accuracy is typically prioritised over speed. Further runtime comparisons with baselines, as well as notes on parallelisation and more detailed practical considerations, are provided in Appendix H.

## 5 Conclusion

In this paper, we propose Decentralized Isolation Networks (DIsoN), a novel OOD detection framework that, unlike most existing methods, actively leverages training data at inference, without requiring data sharing. DIsoN trains a binary classification task to measure the difficulty of isolating a test sample by comparing it to the training data through model parameter exchange between the source and deployment site. Our class-conditional variant, CC-DIsoN, further improves performance and achieves consistent gains in AUROC and FPR95 across four medical imaging datasets and 12 OOD detection tasks, compared to state-of-the-art methods. One limitation of DIsoN is, that it requires additional compute during inference for target samples. In practice, DIsoN requires roughly 40s to 4 min per sample (depending on the dataset), thus it is practical for applications where inference delay of this magnitude is not an issue. We show that this overhead can be controlled via the aggregation weight  $\alpha$  (convergence speed) and backbone size, enabling a trade-off between efficiency and detection performance. In future work, we aim to extend DIsoN to handle multiple target samples simultaneously to improve efficiency. Overall, our results demonstrate that leveraging training data during inference can improve OOD detection in privacy-sensitive deployment scenarios.

## Acknowledgements

FW is supported by the EPSRC Centre for Doctoral Training in Health Data Science (EP/S02428X/1), the Anglo-Austrian Society, and an Oxford-Reuben scholarship. PS is supported by the EPSRC Programme Grant [EP/T028572/1], UKRI grant [EP/X040186/1], and EPSRC Doctoral Training Partnership award. HA is supported by a scholarship via the EPSRC Doctoral Training Partnerships programme [EP/W524311/1, EP/T517811/1]. The authors acknowledge the use of the University of Oxford Advanced Research Computing (ARC) facility (<http://dx.doi.org/10.5281/zenodo.22558>).

## References

- [1] Amorim, J.G.A., Macarini, L.A.B., Matias, A.V., Cerentini, A., Onofre, F.B.D.M., Onofre, A.S.C., Von Wangenheim, A.: A novel approach on segmentation of agnor-stained cytology images using deep learning. In: 2020 IEEE 33rd International Symposium on Computer-Based Medical Systems (CBMS). pp. 552–557. IEEE (2020)
- [2] Anthony, H., Kamnitsas, K.: On the use of mahalanobis distance for out-of-distribution detection with neural networks for medical imaging. In: International Workshop on Uncertainty for Safe Utilization of Machine Learning in Medical Imaging. pp. 136–146. Springer (2023)
- [3] Anthony, H., Kamnitsas, K.: Evaluating reliability in medical dnns: A critical analysis of feature and confidence-based ood detection. In: International Workshop on Uncertainty for Safe Utilization of Machine Learning in Medical Imaging. pp. 160–170. Springer (2024)
- [4] Aubreville, M., Wilm, F., Stathonikos, N., Breininger, K., Donovan, T.A., Jabari, S., Veta, M., Ganz, J., Ammeling, J., van Diest, P.J., et al.: A comprehensive multi-domain dataset for mitotic figure detection. *Scientific data* **10**(1), 484 (2023)
- [5] Blundell, C., Cornebise, J., Kavukcuoglu, K., Wierstra, D.: Weight uncertainty in neural network. In: International conference on machine learning. pp. 1613–1622. PMLR (2015)
- [6] Breunig, M.M., Kriegel, H.P., Ng, R.T., Sander, J.: Lof: identifying density-based local outliers. In: Proceedings of the 2000 ACM SIGMOD international conference on Management of data. pp. 93–104 (2000)
- [7] Chen, J., Qu, X., Li, J., Wang, J., Wan, J., Xiao, J.: Detecting out-of-distribution examples via class-conditional impressions reappearing. In: ICASSP 2023-2023 IEEE International Conference on Acoustics, Speech and Signal Processing (ICASSP). pp. 1–5. IEEE (2023)
- [8] Deng, J., Dong, W., Socher, R., Li, L.J., Li, K., Fei-Fei, L.: Imagenet: A large-scale hierarchical image database. In: 2009 IEEE conference on computer vision and pattern recognition. pp. 248–255. Ieee (2009)
- [9] DeVries, T., Taylor, G.W.: Learning confidence for out-of-distribution detection in neural networks. arXiv preprint arXiv:1802.04865 (2018)
- [10] Fan, K., Liu, T., Qiu, X., Wang, Y., Huai, L., Shangguan, Z., Gou, S., Liu, F., Fu, Y., Fu, Y., et al.: Test-time linear out-of-distribution detection. In: Proceedings of the IEEE/CVF Conference on Computer Vision and Pattern Recognition. pp. 23752–23761 (2024)
- [11] Gutbrod, M., Rauber, D., Nunes, D.W., Palm, C.: Openmibood: Open medical imaging benchmarks for out-of-distribution detection. arXiv preprint arXiv:2503.16247 (2025)
- [12] He, K., Zhang, X., Ren, S., Sun, J.: Deep residual learning for image recognition. In: Proceedings of the IEEE conference on computer vision and pattern recognition. pp. 770–778 (2016)
- [13] Hendrycks, D., Gimpel, K.: A baseline for detecting misclassified and out-of-distribution examples in neural networks. arXiv preprint arXiv:1610.02136 (2016)
- [14] Hendrycks, D., Mazeika, M., Dietterich, T.: Deep anomaly detection with outlier exposure. In: International Conference on Learning Representations (2019)

- [15] Huang, R., Geng, A., Li, Y.: On the importance of gradients for detecting distributional shifts in the wild. *Advances in Neural Information Processing Systems* **34**, 677–689 (2021)
- [16] Ioffe, S., Szegedy, C.: Batch normalization: Accelerating deep network training by reducing internal covariate shift. In: *International conference on machine learning*. pp. 448–456. pmlr (2015)
- [17] Irvin, J., Rajpurkar, P., Ko, M., Yu, Y., Ciurea-Ilicus, S., Chute, C., Marklund, H., Haghighi, B., Ball, R., Shpanskaya, K., et al.: Chexpert: A large chest radiograph dataset with uncertainty labels and expert comparison. In: *Proceedings of the AAAI conference on artificial intelligence*. vol. 33, pp. 590–597 (2019)
- [18] Kamnitsas, K., Winzeck, S., Kornaropoulos, E.N., Whitehouse, D., Englman, C., Phyu, P., Pao, N., Menon, D.K., Rueckert, D., Das, T., et al.: Transductive image segmentation: Self-training and effect of uncertainty estimation. In: *MICCAI Workshop on Domain Adaptation and Representation Transfer*. pp. 79–89. Springer (2021)
- [19] Kawahara, J., Daneshvar, S., Argenziano, G., Hamarneh, G.: Seven-point checklist and skin lesion classification using multitask multimodal neural nets. *IEEE journal of biomedical and health informatics* **23**(2), 538–546 (2018)
- [20] Kingma, D.P., Ba, J.: Adam: A method for stochastic optimization. *arXiv preprint arXiv:1412.6980* (2014)
- [21] Lakshminarayanan, B., Pritzel, A., Blundell, C.: Simple and scalable predictive uncertainty estimation using deep ensembles. *Advances in neural information processing systems* **30** (2017)
- [22] Lee, K., Lee, K., Lee, H., Shin, J.: A simple unified framework for detecting out-of-distribution samples and adversarial attacks. *Advances in neural information processing systems* **31** (2018)
- [23] Liang, S., Li, Y., Srikant, R.: Enhancing the reliability of out-of-distribution image detection in neural networks. *arXiv preprint arXiv:1706.02690* (2017)
- [24] Liao, X., Liu, W., Zhou, P., Yu, F., Xu, J., Wang, J., Wang, W., Chen, C., Zheng, X.: Foogd: Federated collaboration for both out-of-distribution generalization and detection. *arXiv preprint arXiv:2410.11397* (2024)
- [25] Liu, F.T., Ting, K.M., Zhou, Z.H.: Isolation forest. In: *2008 eighth IEEE international conference on data mining*. pp. 413–422. IEEE (2008)
- [26] Liu, L., Qin, Y.: Fast decision boundary based out-of-distribution detector. In: *International Conference on Machine Learning*. pp. 31728–31746. PMLR (2024)
- [27] Liu, W., Wang, X., Owens, J., Li, Y.: Energy-based out-of-distribution detection. *Advances in neural information processing systems* **33**, 21464–21475 (2020)
- [28] Liu, W., Wang, X., Owens, J., Li, Y.: Energy-based out-of-distribution detection. *Advances in neural information processing systems* **33**, 21464–21475 (2020)
- [29] Lu, H., Gong, D., Wang, S., Xue, J., Yao, L., Moore, K.: Learning with mixture of prototypes for out-of-distribution detection. In: *The Twelfth International Conference on Learning Representations* (2024)
- [30] Ming, Y., Sun, Y., Dia, O., Li, Y.: How to exploit hyperspherical embeddings for out-of-distribution detection? In: *The Eleventh International Conference on Learning Representations* (2023)
- [31] NHS-England: Diagnostic imaging reporting turnaround times. <https://www.england.nhs.uk/long-read/diagnostic-imaging-reporting-turnaround-times/>, accessed: 2025-08-20
- [32] Saikia, A.R., Bora, K., Mahanta, L.B., Das, A.K.: Comparative assessment of cnn architectures for classification of breast fnac images. *Tissue and Cell* **57**, 8–14 (2019)

- [33] Shome, D., Kar, T.: Fedaffect: Few-shot federated learning for facial expression recognition. In: Proceedings of the IEEE/CVF international conference on computer vision workshops. pp. 4168–4175 (2021)
- [34] Sun, Y., Ming, Y., Zhu, X., Li, Y.: Out-of-distribution detection with deep nearest neighbors. In: International Conference on Machine Learning. pp. 20827–20840. PMLR (2022)
- [35] Ulyanov, D., Vedaldi, A., Lempitsky, V.: Instance normalization: The missing ingredient for fast stylization. arXiv preprint arXiv:1607.08022 (2016)
- [36] Van Amersfoort, J., Smith, L., Teh, Y.W., Gal, Y.: Uncertainty estimation using a single deep deterministic neural network. In: International conference on machine learning. pp. 9690–9700. PMLR (2020)
- [37] Wang, H., Li, Z., Feng, L., Zhang, W.: Vim: Out-of-distribution with virtual-logit matching. In: Proceedings of the IEEE/CVF conference on computer vision and pattern recognition. pp. 4921–4930 (2022)
- [38] Wang, S., Fu, X., Ding, K., Chen, C., Chen, H., Li, J.: Federated few-shot learning. In: Proceedings of the 29th ACM SIGKDD Conference on Knowledge Discovery and Data Mining. pp. 2374–2385 (2023)
- [39] Wen, Y., Vicol, P., Ba, J., Tran, D., Grosse, R.: Flipout: Efficient pseudo-independent weight perturbations on mini-batches. arXiv preprint arXiv:1803.04386 (2018)
- [40] Xu, H., Pang, G., Wang, Y., Wang, Y.: Deep isolation forest for anomaly detection. IEEE Transactions on Knowledge and Data Engineering **35**(12), 12591–12604 (2023)
- [41] Yang, J., Shi, R., Wei, D., Liu, Z., Zhao, L., Ke, B., Pfister, H., Ni, B.: Medmnist v2-a large-scale lightweight benchmark for 2d and 3d biomedical image classification. Scientific Data **10**(1), 41 (2023)
- [42] Yang, J., Wang, P., Zou, D., Zhou, Z., Ding, K., Peng, W., Wang, H., Chen, G., Li, B., Sun, Y., et al.: Openood: Benchmarking generalized out-of-distribution detection. Advances in Neural Information Processing Systems **35**, 32598–32611 (2022)
- [43] Yang, J., Zhou, K., Li, Y., Liu, Z.: Generalized out-of-distribution detection: A survey. International Journal of Computer Vision **132**(12), 5635–5662 (2024)
- [44] Yu, S., Hong, J., Wang, H., Wang, Z., Zhou, J.: Turning the curse of heterogeneity in federated learning into a blessing for out-of-distribution detection. In: 2023 International Conference on Learning Representations (2023)

## NeurIPS Paper Checklist

### 1. Claims

Question: Do the main claims made in the abstract and introduction accurately reflect the paper's contributions and scope?

Answer: [Yes]

Justification: Yes. Our main contributions are detailed in Sec. 1. See Sec.3 for our method description and Sec.4 for experimental evidence.

Guidelines:

- The answer NA means that the abstract and introduction do not include the claims made in the paper.
- The abstract and/or introduction should clearly state the claims made, including the contributions made in the paper and important assumptions and limitations. A No or NA answer to this question will not be perceived well by the reviewers.
- The claims made should match theoretical and experimental results, and reflect how much the results can be expected to generalize to other settings.
- It is fine to include aspirational goals as motivation as long as it is clear that these goals are not attained by the paper.

### 2. Limitations

Question: Does the paper discuss the limitations of the work performed by the authors?

Answer: [Yes]

Justification: Yes. Please see Sec.5, where we discuss limitations and future research plans.

Guidelines:

- The answer NA means that the paper has no limitation while the answer No means that the paper has limitations, but those are not discussed in the paper.
- The authors are encouraged to create a separate "Limitations" section in their paper.
- The paper should point out any strong assumptions and how robust the results are to violations of these assumptions (e.g., independence assumptions, noiseless settings, model well-specification, asymptotic approximations only holding locally). The authors should reflect on how these assumptions might be violated in practice and what the implications would be.
- The authors should reflect on the scope of the claims made, e.g., if the approach was only tested on a few datasets or with a few runs. In general, empirical results often depend on implicit assumptions, which should be articulated.
- The authors should reflect on the factors that influence the performance of the approach. For example, a facial recognition algorithm may perform poorly when image resolution is low or images are taken in low lighting. Or a speech-to-text system might not be used reliably to provide closed captions for online lectures because it fails to handle technical jargon.
- The authors should discuss the computational efficiency of the proposed algorithms and how they scale with dataset size.
- If applicable, the authors should discuss possible limitations of their approach to address problems of privacy and fairness.
- While the authors might fear that complete honesty about limitations might be used by reviewers as grounds for rejection, a worse outcome might be that reviewers discover limitations that aren't acknowledged in the paper. The authors should use their best judgment and recognize that individual actions in favor of transparency play an important role in developing norms that preserve the integrity of the community. Reviewers will be specifically instructed to not penalize honesty concerning limitations.

### 3. Theory assumptions and proofs

Question: For each theoretical result, does the paper provide the full set of assumptions and a complete (and correct) proof?

Answer: [Yes]

Justification: Yes. Sec.3.2 includes a Proposition with its proof sketch. The full proof can be found in the Appendix.

Guidelines:

- The answer NA means that the paper does not include theoretical results.
- All the theorems, formulas, and proofs in the paper should be numbered and cross-referenced.
- All assumptions should be clearly stated or referenced in the statement of any theorems.
- The proofs can either appear in the main paper or the supplemental material, but if they appear in the supplemental material, the authors are encouraged to provide a short proof sketch to provide intuition.
- Inversely, any informal proof provided in the core of the paper should be complemented by formal proofs provided in appendix or supplemental material.
- Theorems and Lemmas that the proof relies upon should be properly referenced.

#### 4. Experimental result reproducibility

Question: Does the paper fully disclose all the information needed to reproduce the main experimental results of the paper to the extent that it affects the main claims and/or conclusions of the paper (regardless of whether the code and data are provided or not)?

Answer: [Yes]

Justification: Yes. Sec.3 includes a detailed description of our method. Sec.4 includes a description of the hyperparameters. we also use publicly available datasets. A more detailed hyperparameter description is included in the Appendix. We also upload the code.

Guidelines:

- The answer NA means that the paper does not include experiments.
- If the paper includes experiments, a No answer to this question will not be perceived well by the reviewers: Making the paper reproducible is important, regardless of whether the code and data are provided or not.
- If the contribution is a dataset and/or model, the authors should describe the steps taken to make their results reproducible or verifiable.
- Depending on the contribution, reproducibility can be accomplished in various ways. For example, if the contribution is a novel architecture, describing the architecture fully might suffice, or if the contribution is a specific model and empirical evaluation, it may be necessary to either make it possible for others to replicate the model with the same dataset, or provide access to the model. In general, releasing code and data is often one good way to accomplish this, but reproducibility can also be provided via detailed instructions for how to replicate the results, access to a hosted model (e.g., in the case of a large language model), releasing of a model checkpoint, or other means that are appropriate to the research performed.
- While NeurIPS does not require releasing code, the conference does require all submissions to provide some reasonable avenue for reproducibility, which may depend on the nature of the contribution. For example
  - (a) If the contribution is primarily a new algorithm, the paper should make it clear how to reproduce that algorithm.
  - (b) If the contribution is primarily a new model architecture, the paper should describe the architecture clearly and fully.
  - (c) If the contribution is a new model (e.g., a large language model), then there should either be a way to access this model for reproducing the results or a way to reproduce the model (e.g., with an open-source dataset or instructions for how to construct the dataset).
  - (d) We recognize that reproducibility may be tricky in some cases, in which case authors are welcome to describe the particular way they provide for reproducibility. In the case of closed-source models, it may be that access to the model is limited in some way (e.g., to registered users), but it should be possible for other researchers to have some path to reproducing or verifying the results.

#### 5. Open access to data and code

Question: Does the paper provide open access to the data and code, with sufficient instructions to faithfully reproduce the main experimental results, as described in supplemental material?

Answer: [Yes]

Justification: We use publicly available datasets as described in Sec.4. We also upload the code and once the review process is finished, we will open source the code and instructions.

Guidelines:

- The answer NA means that paper does not include experiments requiring code.
- Please see the NeurIPS code and data submission guidelines (<https://nips.cc/public/guides/CodeSubmissionPolicy>) for more details.
- While we encourage the release of code and data, we understand that this might not be possible, so “No” is an acceptable answer. Papers cannot be rejected simply for not including code, unless this is central to the contribution (e.g., for a new open-source benchmark).
- The instructions should contain the exact command and environment needed to run to reproduce the results. See the NeurIPS code and data submission guidelines (<https://nips.cc/public/guides/CodeSubmissionPolicy>) for more details.
- The authors should provide instructions on data access and preparation, including how to access the raw data, preprocessed data, intermediate data, and generated data, etc.
- The authors should provide scripts to reproduce all experimental results for the new proposed method and baselines. If only a subset of experiments are reproducible, they should state which ones are omitted from the script and why.
- At submission time, to preserve anonymity, the authors should release anonymized versions (if applicable).
- Providing as much information as possible in supplemental material (appended to the paper) is recommended, but including URLs to data and code is permitted.

## 6. Experimental setting/details

Question: Does the paper specify all the training and test details (e.g., data splits, hyperparameters, how they were chosen, type of optimizer, etc.) necessary to understand the results?

Answer: [Yes]

Justification: Yes. Sec.4 describes the training details, including hyperparameters, type of optimizer and dataset splits. A more detailed description about the training and test details is provided in the Appendix.

Guidelines:

- The answer NA means that the paper does not include experiments.
- The experimental setting should be presented in the core of the paper to a level of detail that is necessary to appreciate the results and make sense of them.
- The full details can be provided either with the code, in appendix, or as supplemental material.

## 7. Experiment statistical significance

Question: Does the paper report error bars suitably and correctly defined or other appropriate information about the statistical significance of the experiments?

Answer: [Yes]

Justification: We now report mean and standard deviation over three random seeds for our main experiments (added after rebuttal). In Table 1 we show mean and standard deviation. For the larger Histopathology table (Table 2) we show means in the main text and include the corresponding standard deviations in Appendix I (Tables 13 and 14). Additionally, our method is evaluated across multiple diverse medical datasets and tasks (Sec. 4).

Guidelines:

- The answer NA means that the paper does not include experiments.

- The authors should answer "Yes" if the results are accompanied by error bars, confidence intervals, or statistical significance tests, at least for the experiments that support the main claims of the paper.
- The factors of variability that the error bars are capturing should be clearly stated (for example, train/test split, initialization, random drawing of some parameter, or overall run with given experimental conditions).
- The method for calculating the error bars should be explained (closed form formula, call to a library function, bootstrap, etc.)
- The assumptions made should be given (e.g., Normally distributed errors).
- It should be clear whether the error bar is the standard deviation or the standard error of the mean.
- It is OK to report 1-sigma error bars, but one should state it. The authors should preferably report a 2-sigma error bar than state that they have a 96% CI, if the hypothesis of Normality of errors is not verified.
- For asymmetric distributions, the authors should be careful not to show in tables or figures symmetric error bars that would yield results that are out of range (e.g. negative error rates).
- If error bars are reported in tables or plots, The authors should explain in the text how they were calculated and reference the corresponding figures or tables in the text.

#### 8. Experiments compute resources

Question: For each experiment, does the paper provide sufficient information on the computer resources (type of compute workers, memory, time of execution) needed to reproduce the experiments?

Answer: [Yes]

Justification: Sec. 4 describes the type of GPU that was used for our experiments. With this GPU type, all of our experiments can be executed.

Guidelines:

- The answer NA means that the paper does not include experiments.
- The paper should indicate the type of compute workers CPU or GPU, internal cluster, or cloud provider, including relevant memory and storage.
- The paper should provide the amount of compute required for each of the individual experimental runs as well as estimate the total compute.
- The paper should disclose whether the full research project required more compute than the experiments reported in the paper (e.g., preliminary or failed experiments that didn't make it into the paper).

#### 9. Code of ethics

Question: Does the research conducted in the paper conform, in every respect, with the NeurIPS Code of Ethics [https://neurips.cc/public/EthicsGuidelines?](https://neurips.cc/public/EthicsGuidelines)

Answer: [Yes]

Justification: Yes. Our research conforms with the NeurIPS Code of Ethics.

Guidelines:

- The answer NA means that the authors have not reviewed the NeurIPS Code of Ethics.
- If the authors answer No, they should explain the special circumstances that require a deviation from the Code of Ethics.
- The authors should make sure to preserve anonymity (e.g., if there is a special consideration due to laws or regulations in their jurisdiction).

#### 10. Broader impacts

Question: Does the paper discuss both potential positive societal impacts and negative societal impacts of the work performed?

Answer: [Yes]

Justification: Our research is intended to have a potential positive societal impact in medical imaging as discussed in the paper. The paper mentions possible negative impacts if OOD methods do not work.

Guidelines:

- The answer NA means that there is no societal impact of the work performed.
- If the authors answer NA or No, they should explain why their work has no societal impact or why the paper does not address societal impact.
- Examples of negative societal impacts include potential malicious or unintended uses (e.g., disinformation, generating fake profiles, surveillance), fairness considerations (e.g., deployment of technologies that could make decisions that unfairly impact specific groups), privacy considerations, and security considerations.
- The conference expects that many papers will be foundational research and not tied to particular applications, let alone deployments. However, if there is a direct path to any negative applications, the authors should point it out. For example, it is legitimate to point out that an improvement in the quality of generative models could be used to generate deepfakes for disinformation. On the other hand, it is not needed to point out that a generic algorithm for optimizing neural networks could enable people to train models that generate Deepfakes faster.
- The authors should consider possible harms that could arise when the technology is being used as intended and functioning correctly, harms that could arise when the technology is being used as intended but gives incorrect results, and harms following from (intentional or unintentional) misuse of the technology.
- If there are negative societal impacts, the authors could also discuss possible mitigation strategies (e.g., gated release of models, providing defenses in addition to attacks, mechanisms for monitoring misuse, mechanisms to monitor how a system learns from feedback over time, improving the efficiency and accessibility of ML).

## 11. Safeguards

Question: Does the paper describe safeguards that have been put in place for responsible release of data or models that have a high risk for misuse (e.g., pretrained language models, image generators, or scraped datasets)?

Answer: [NA]

Justification: We do not expect a high risk of misuse of this work.

Guidelines:

- The answer NA means that the paper poses no such risks.
- Released models that have a high risk for misuse or dual-use should be released with necessary safeguards to allow for controlled use of the model, for example by requiring that users adhere to usage guidelines or restrictions to access the model or implementing safety filters.
- Datasets that have been scraped from the Internet could pose safety risks. The authors should describe how they avoided releasing unsafe images.
- We recognize that providing effective safeguards is challenging, and many papers do not require this, but we encourage authors to take this into account and make a best faith effort.

## 12. Licenses for existing assets

Question: Are the creators or original owners of assets (e.g., code, data, models), used in the paper, properly credited and are the license and terms of use explicitly mentioned and properly respected?

Answer: [Yes]

Justification: Yes, we credited them properly.

Guidelines:

- The answer NA means that the paper does not use existing assets.
- The authors should cite the original paper that produced the code package or dataset.

- The authors should state which version of the asset is used and, if possible, include a URL.
- The name of the license (e.g., CC-BY 4.0) should be included for each asset.
- For scraped data from a particular source (e.g., website), the copyright and terms of service of that source should be provided.
- If assets are released, the license, copyright information, and terms of use in the package should be provided. For popular datasets, [paperswithcode.com/datasets](https://paperswithcode.com/datasets) has curated licenses for some datasets. Their licensing guide can help determine the license of a dataset.
- For existing datasets that are re-packaged, both the original license and the license of the derived asset (if it has changed) should be provided.
- If this information is not available online, the authors are encouraged to reach out to the asset's creators.

### 13. **New assets**

Question: Are new assets introduced in the paper well documented and is the documentation provided alongside the assets?

Answer: [NA]

Justification: Our work does not release new assets.

Guidelines:

- The answer NA means that the paper does not release new assets.
- Researchers should communicate the details of the dataset/code/model as part of their submissions via structured templates. This includes details about training, license, limitations, etc.
- The paper should discuss whether and how consent was obtained from people whose asset is used.
- At submission time, remember to anonymize your assets (if applicable). You can either create an anonymized URL or include an anonymized zip file.

### 14. **Crowdsourcing and research with human subjects**

Question: For crowdsourcing experiments and research with human subjects, does the paper include the full text of instructions given to participants and screenshots, if applicable, as well as details about compensation (if any)?

Answer: [NA]

Justification: Our paper does not involve crowdsourcing and human subjects.

Guidelines:

- The answer NA means that the paper does not involve crowdsourcing nor research with human subjects.
- Including this information in the supplemental material is fine, but if the main contribution of the paper involves human subjects, then as much detail as possible should be included in the main paper.
- According to the NeurIPS Code of Ethics, workers involved in data collection, curation, or other labor should be paid at least the minimum wage in the country of the data collector.

### 15. **Institutional review board (IRB) approvals or equivalent for research with human subjects**

Question: Does the paper describe potential risks incurred by study participants, whether such risks were disclosed to the subjects, and whether Institutional Review Board (IRB) approvals (or an equivalent approval/review based on the requirements of your country or institution) were obtained?

Answer: [NA]

Justification: Our paper does not involve crowdsourcing and human subjects.

Guidelines:

- The answer NA means that the paper does not involve crowdsourcing nor research with human subjects.
- Depending on the country in which research is conducted, IRB approval (or equivalent) may be required for any human subjects research. If you obtained IRB approval, you should clearly state this in the paper.
- We recognize that the procedures for this may vary significantly between institutions and locations, and we expect authors to adhere to the NeurIPS Code of Ethics and the guidelines for their institution.
- For initial submissions, do not include any information that would break anonymity (if applicable), such as the institution conducting the review.

**16. Declaration of LLM usage**

Question: Does the paper describe the usage of LLMs if it is an important, original, or non-standard component of the core methods in this research? Note that if the LLM is used only for writing, editing, or formatting purposes and does not impact the core methodology, scientific rigorousness, or originality of the research, declaration is not required.

Answer: [NA]

Justification: LLMs were not an important, original, or non-standard component of our research.

Guidelines:

- The answer NA means that the core method development in this research does not involve LLMs as any important, original, or non-standard components.
- Please refer to our LLM policy (<https://neurips.cc/Conferences/2025/LLM>) for what should or should not be described.

## A DIsoN and CC-DIsoN: Algorithm

In this section, we present pseudocode for our DIsoN method and its class-conditional variant, CC-DIsoN. Algorithm 1 describes the code that is executed on the Source Node, while Algorithm 2 runs on the Target Node. Lines specific to CC-DIsoN are highlighted in blue. The **initialization step** occurs in lines 4–5 of Algorithm 1 and line 5 of Algorithm 2. The **local updates** step is performed on lines 7–12 (Source) and 7–8 (Target), followed by the **aggregation step** on line 14 on the Source Node. If the convergence criteria (Def. 3.1) are not met, another communication round starts.

The algorithms demonstrate that implementing CC-DIsoN requires only minor changes compared to DIsoN: before initialization, the Target Node predicts the target sample’s class using the pre-trained model and sends it to the Source Node (lines 2–4 of Algorithm 2). The Source Node then filters its training data to sample batches from the predicted class *only* (line 9 of Algorithm 1).

---

**Algorithm 1** Source Node: DIsoN / CC-DIsoN

---

```

1: function SOURCENODE( $\mathcal{D}_s$ ,  $\theta^{\text{pre}}$ )
2:   if CC-DIsoN :
3:     receive  $\hat{y}$  from target
4:      $\theta^f \leftarrow \theta^{\text{pre}}$ ;  $\theta^h \leftarrow \text{rand}$ ;  $\theta^{(0)} \leftarrow (\theta^f, \theta^h)$            ▷ initialize global model
5:     send  $\theta^{(0)}$  to Target;  $\theta_S \leftarrow \theta^{(0)}$ 
6:     for  $r = 1$  to  $R$  do                                           ▷ communication rounds
7:       for  $e = 1$  to  $E$  do                                           ▷ local updates on Source
8:         if CC-DIsoN :
9:            $B_s \sim \{(\mathbf{x}_s, y_s) \in \mathcal{D}_s \mid y_s = \hat{y}\}$            ▷ filter  $B_s$  on predicted  $\mathbf{x}_t$  class
10:        else
11:          sample  $B_s \sim \mathcal{D}_s$ 
12:           $\theta_S \leftarrow \theta_S - \eta \nabla_{\theta_S} [\frac{1}{|B_s|} \sum_{\mathbf{x}_s \in B_s} L(\theta_S; \mathbf{x}_s, 0)]$ 
13:        receive  $\theta_T$  from Target
14:        aggregation:  $\theta^{(r)} \leftarrow \alpha \theta_S + (1 - \alpha) \theta_T$            ▷ Eq. 2
15:        SourceConverged  $\leftarrow \text{converged}(\theta^{(r)}, \mathcal{D}_s)$            ▷ Test criteria 2 (Def. 3.1)
16:        send  $\theta^{(r)}$  and SourceConverged to Target
17:         $\theta_S \leftarrow \theta^{(r)}$            ▷ update Source model for next comm. round

```

---



---

**Algorithm 2** Target Node: DIsoN / CC-DIsoN

---

```

1: function TARGETNODE( $x_t$ ,  $M_{\text{pre}}$ ,  $R$ )
2:   if CC-DIsoN :
3:      $\hat{y} \leftarrow \arg \max_c [M_{\text{pre}}(\mathbf{x}_t)]_c$ 
4:     send  $\hat{y}$  to source
5:   receive  $\theta^{(0)}$  from Source;  $\theta_T \leftarrow \theta^{(0)}$            ▷ init. Target model with global model
6:   for  $r = 1$  to  $R$  do                                           ▷ communication rounds
7:     for  $e = 1$  to  $E$  do                                           ▷ local updates on Target
8:        $\theta_T \leftarrow \theta_T - \eta \nabla_{\theta_T} L(\theta_T; \mathbf{x}_t, 1)$ 
9:     send  $\theta_T$  to Source
10:    receive updated  $\theta^{(r)}$  and SourceConverged from Source
11:    if converged( $\theta^{(r)}, \mathbf{x}_t$ ) and SourceConverged: ▷ Test crit. 1 & 2 (Def. 3.1)
12:      break
13:     $\theta_T \leftarrow \theta^{(r)}$            ▷ update Target model for next comm. round
14:  return  $S_{\text{DIsoN}}(\mathbf{x}_t) = r$ 

```

---

## B Connection between DIsoN and Isolation Network: Proof Proposition 3.1

This section provides the full proof of Proposition 3.1, which states that if we set  $E = 1$  and the aggregation weights in Eq. 2 accordingly, DIsoN becomes equivalent to the centralized Isolation

Network. This result also demonstrates how the aggregation weight  $\alpha$  implicitly controls the number of times the target sample is oversampled ( $N$ ) in Eq. 1 for the Isolation Network.

We begin by restating Proposition 3.1:

**Proposition 3.1** (DIsoN and Centralized Isolation Network Equivalence for  $E = 1$ ). *Let  $\theta_{cent}$  be the model parameters from our centralized algorithm and  $\theta_{dec}$  be the parameters from DIsoN. Let each site perform one local SGD step ( $E = 1$ ) with learning rate  $\eta$ , and aggregate with  $\alpha = \frac{|B_s|}{|B_s|+N}$ ,  $\beta = \frac{N}{|B_s|+N}$ . Then the decentralized update equals the centralized one:*

$$\theta_{dec}^{(r+1)} = \theta^{(r)} - \eta(\alpha g_S(\theta^{(r)}) + \beta g_T(\theta^{(r)})) = \theta^{(r)} - \eta g_c(\theta^{(r)}) = \theta_{cent}^{(r+1)},$$

where  $g_S(\theta) = \frac{1}{|B_s|} \sum_{\mathbf{x}_s \in B_s} \nabla_{\theta} L(\theta; \mathbf{x}_s, 0)$ ,  $g_T(\theta) = \nabla_{\theta} L(\theta; \mathbf{x}_t, 1)$  and  $N$  is the number of times  $\mathbf{x}_t$  is oversampled in the centralized version.

*Proof.* Recall that  $B_s$  is a mini-batch of  $|B_s|$  source samples and let the target sample  $\mathbf{x}_t$  be oversampled  $N$  times in the Isolation Network. The local gradient on the source node  $g_S$  and on the target node  $g_T$  are defined as:

$$g_S(\theta) = \frac{1}{|B_s|} \sum_{\mathbf{x}_s \in B_s} \nabla_{\theta} L(\theta; \mathbf{x}_s, 0), \quad g_T(\theta) = \nabla_{\theta} L(\theta; \mathbf{x}_t, 1),$$

and the *centralized* mini-batch gradient of the Isolation Network is defined as:

$$g_c(\theta) = \frac{1}{|B_s| + N} \left( \sum_{\mathbf{x}_s \in B_s} \nabla_{\theta} L(\theta; \mathbf{x}_s, 0) + N \cdot \nabla_{\theta} L(\theta; \mathbf{x}_t, 1) \right). \quad (\text{A.1})$$

**Step 1. Local parameter updates on the Source Node and Target Node.** After one SGD step ( $E = 1$ ) with learning rate  $\eta$  we have,

$$\theta_S^{(r,1)} = \theta^{(r)} - \eta g_S(\theta^{(r)}), \quad \theta_T^{(r,1)} = \theta^{(r)} - \eta g_T(\theta^{(r)}). \quad (\text{A.2})$$

**Step 2. Weighted aggregation.** Using the aggregation Eq. 2 with  $\alpha = \frac{|B_s|}{|B_s| + N}$ ,  $\beta = \frac{N}{|B_s| + N}$ ,  $\beta = 1 - \alpha$  gives

$$\begin{aligned} \theta_{dec}^{(r+1)} &= \alpha \theta_S^{(r,1)} + \beta \theta_T^{(r,1)} \\ &= \alpha(\theta^{(r)} - \eta g_S) + \beta(\theta^{(r)} - \eta g_T) \quad (\text{by (A.2)}) \\ &= (\alpha + \beta)\theta^{(r)} - \eta(\alpha g_S + \beta g_T) \\ &= \theta^{(r)} - \eta(\alpha g_S + \beta g_T). \end{aligned} \quad (\text{A.3})$$

**Step 3. Centralized gradient of the Isolation Network.**

$$\begin{aligned} \alpha g_S &= \frac{|B_s|}{|B_s| + N} \left( \frac{1}{|B_s|} \sum_{\mathbf{x}_s \in B_s} \nabla_{\theta} L(\theta; \mathbf{x}_s, 0) \right) = \frac{1}{|B_s| + N} \sum_{\mathbf{x}_s \in B_s} \nabla_{\theta} L(\theta; \mathbf{x}_s, 0), \\ \beta g_T &= \frac{N}{|B_s| + N} \nabla_{\theta} L(\theta; \mathbf{x}_t, 1). \end{aligned}$$

Adding the two terms reproduces (A.1):

$$\alpha g_S + \beta g_T = \frac{1}{|B_s| + N} \left( \sum_{\mathbf{x}_s \in B_s} \nabla_{\theta} L(\theta; \mathbf{x}_s, 0) + N \nabla_{\theta} L(\theta; \mathbf{x}_t, 1) \right) = g_c(\theta). \quad (\text{A.4})$$

**Step 4. Equality of parameter updates.** Substituting (A.4) into (A.3) results in

$$\theta_{dec}^{(r+1)} = \theta^{(r)} - \eta g_c(\theta^{(r)}) = \theta_{cent}^{(r+1)}, \quad (\text{A.5})$$

which is exactly the centralized Isolation Network SGD update. This shows that the decentralized and centralized updates are equivalent when  $E = 1$  and the aggregation weights are chosen as  $\alpha = \frac{|B_s|}{|B_s|+N}$ ,  $\beta = \frac{N}{|B_s|+N}$ .

□

Table 4: Class-wise dataset splits used in our experiments, showing the total number of ID images per class, splits into pre-training and ID test sets, OOD detection task, number of OOD test samples, and image resolution. For Histopathology, we report near-OOD (domains 2–7) and far-OOD (CCAgT, FNAC 2019) tasks separately.

Dataset	Class	Total: # ID Images	Pre-train: # Images	# ID Test	OOD Task	# OOD Test	Img. Size
Dermatology	Nevus	832	745	87	black ruler	251	224×224
	Not Nevus	571	516	55			
Ultrasound	Normal	126	114	12	text annotations	228	224×224
	Benign	269	245	24			
	Malignant	157	137	20			
Chest X-Ray	Cardiomegaly	1788	1711	77	pacemaker	1000	224×224
	No Cardiomegaly	21557	20634	923			
Histopathology	Mitotic	421	375	46	near-OOD: domains 2–7	500 per domain	50×50
	Imposter	663	581	82			
	Neither	1063	940	123	far-OOD: CCAgT & FNAC		

## C Dataset Details.

We evaluate DIsOn on four medical imaging datasets with two main OOD settings: (i) **artifact detection** (Dermatology, Breast Ultrasound, Chest X-ray) and (ii) **semantic/covariate shift detection** (Histopathology). In this section, we provide more detailed dataset information with class-wise splits used in our experiments. Table 4 reports the total number of images per class, splits into pre-training and ID test samples, the number of OOD test samples, the OOD task and the image size.

For Dermatology (1403 artifact-free ID images) and Breast Ultrasound (552 artifact-free ID images), we follow the benchmark setup from [3], using manually annotated artifact-free images for pre-training and ID testing, and ruler/text annotation artifacts as OOD. The Chest X-ray dataset uses 23,345 frontal-view scans without support devices as ID data, following the setup from [2], with scans with pacemakers as OOD artifacts. In all three datasets, the ID data is split 90/10 into pre-training for the main task of interest and ID test sets.

For Histopathology, we follow the recently published OpenMIBOOD [11] benchmark, which uses a similar setup to the well-known OpenOOD benchmark [42], but is specialized on medical images. OpenMIBOOD demonstrates that many state-of-the-art OOD detection methods fail to generalize to medical data. The dataset is split into multiple domains. The dataset consists of Hematoxylin & Eosin-stained histology patches grouped into multiple domains. Following the protocol in [11], we use the training split of domain 1a (1,896 ID images) for pre-training and its test split (251 images) as the ID evaluation set.

Domains 2–7 are treated as near-OOD and include seven distinct cancer types (breast carcinoma, lung carcinoma, lymphosarcoma, cutaneous mast cell tumor, neuroendocrine tumor, soft tissue sarcoma, and melanoma), from both human and canine. These domains introduce semantic shifts in cell types as well as covariate shifts due to different staining protocols and imaging hardware. For far-OOD, two external datasets are used, that introduce a strong semantic shift: CCAgT [1], which uses AgNOR staining, and FNAC 2019 [32], which uses Pap staining, both differ significantly from the Hematoxylin & Eosin staining used for ID data and are also used for different medical applications.

## D Training Details & Hyperparameters

In addition to the training details provided in Section 4, this section presents further training details and hyperparameters.

Table 5: **Pre-training hyperparameters.** These settings are used to train the main classification task before initializing DIsOn. LR: learning rate; BS: batch size.

Dataset	Main Task	Arch.	Optim.	Epochs	LR	BS
Dermatology	Nevus vs. Non-Nevus	ResNet18	Adam	750	$1 \times 10^{-3}$	32
Breast Ultrasound	Normal / Benign / Malignant	ResNet18	Adam	1000	$1 \times 10^{-3}$	32
Chest X-Ray	Cardiomegaly vs. No Cardiomegaly	ResNet18	Adam	500	$1 \times 10^{-3}$	32
Histopathology	Mitotic / Imposter / Neither	ResNet18	SGD (0.9 momentum)	300	$5 \times 10^{-4}$	128

Table 6: **Training hyperparameters used for DIsoN experiments.** Overview of architecture, optimizer, learning rate (LR), and batch size (BS) used to train DIsoN for each dataset.

Dataset	Arch.	Optim.	LR	BS
Dermatology	ResNet18	Adam	$1 \times 10^{-3}$	16
Breast Ultrasound	ResNet18	Adam	$1 \times 10^{-3}$	8
Chest X-Ray	ResNet18	Adam	$3 \times 10^{-3}$	16
Histopathology	ResNet18	Adam	$1 \times 10^{-2}$	16

### D.1 Pre-Training for the Main Task of Interest

We pre-train a ResNet18 on each dataset’s main classification task. DIsoN models use Instance Normalization, as described in Section 3. For baseline methods, we use Batch Normalization (BN) to ensure a fair comparison, since they assume BN in their original setups. Table 5 summarizes the training settings, using the dataset split in the “Pre-train” column of Table 4. For the Histopathology dataset, we follow the protocol from [11], initializing with ImageNet-1k [8] pre-trained weights to reduce training time, and use SGD with momentum. All other models are trained from scratch using Adam.

### D.2 Training DIsoN

This subsection provides a more detailed description of the DIsoN training setup introduced in Section 4. Table 6 summarizes the training hyperparameters. The Source Node uses the pre-training split from Table 4 as its training data. As described earlier, we set the number of local iterations per communication round such that it approximately matches one epoch over the training data. To limit runtime, we also use a maximum number of communication rounds for each dataset. If convergence is not reached within this limit, we assign the maximum round  $R_{\max}$  as the OOD score. We use  $R_{\max} = 300$  for Dermatology and Ultrasound, and  $R_{\max} = 100$  for the longer-running Chest X-ray and Histopathology datasets.

**Image Augmentations.** As described in Section 3, we apply standard stochastic image augmentations across all datasets. The augmentations for each dataset are mostly identical, with only minor dataset-specific adjustments. For Histopathology, due to the smaller image size, we reduce the rotation range and leave out random cropping. For Breast Ultrasound, we replace random cropping with color jitter. The full set of augmentations are listed below:

- **Random rotation:**  $\pm 15^\circ$  (use  $\pm 5^\circ$  for Histopathology)
- **Random crop:**  $224 \times 224$  with padding=25 (applied to Chest X-Ray & Dermatology)
- **Color jitter:** brightness=0.1, contrast=0.1 (applied to Breast Ultrasound)

**Convergence Parameter Choices for  $E_{\text{stab}}$  and  $\tau$ .** The parameters  $E_{\text{stab}}$  and  $\tau$  were chosen to capture the convergence behavior of the isolation process. Specifically,  $E_{\text{stab}}$  acts as a patience parameter, conceptually similar to early-stopping criteria in learning-rate schedulers, requiring correct classification of  $\mathbf{x}_t$  for several consecutive rounds to ensure stable convergence. We set  $E_{\text{stab}} = 5$ , a commonly used value in schedulers that effectively captures convergence. The confidence threshold  $\tau = 0.85$  ensures that the model learned to separate the target sample with sufficient confidence. This value follows standard practice in uncertainty-based literature [18]. In preliminary experiments, these values consistently produced stable and reliable results, so they were kept fixed across all datasets to avoid dataset-specific tuning or overfitting.

**Effect of partial Fine-Tuning** We also examined whether freezing parts of the network could be beneficial for the isolation task by simplifying optimization. Freezing the backbone, however, assumes that the pre-trained feature extractor already provides sufficiently expressive embeddings to distinguish ID from OOD samples. We found this assumption too restrictive: in early experiments, partial fine-tuning of the network (e.g., only the head or last block) led to worse OOD detection performance than fine-tuning the entire model.

## E Additional Details: Ablation Study for Impact of Predicted Class Accuracies for Class-Conditional Sampling

CC-DIsoN uses predictions of a primary model  $M_{\text{pre}}$ , deployed for a task of interest (e.g., cardiomegaly classification in X-rays; see Sec. 4), for class-conditional sampling. This enables comparing a target sample to the most relevant subset of training data (its predicted class) rather than to all training samples. Our ablations on the effects of class-conditioning (Tab. 3a) demonstrated that class-conditional sampling improves OOD detection performance, while DIsoN without class-conditioning still performs well (see comparison between Tabs. 3a and 1).

To further analyze the influence of class-conditioning and how misclassifications affect the results, we provide here a more detailed analysis of the ablation study on predicted class accuracy introduced in Section 4.1. We first measure the classification accuracy of  $M_{\text{pre}}$  on ID, OOD, and combined target samples, along with the corresponding CC-DIsoN AUROC scores (Tab. 7). Typically, especially in safety-critical domains such as healthcare, high ID accuracy is a requirement for deployment. It is also expected that classification accuracy decreases on OOD samples due to domain shift. Comparing these accuracies with OOD detection performance shows no clear correlation, for example, the Dermatology dataset achieves the highest AUROC (89.5) despite the lowest classification accuracy (63.0%). This indicates that CC-DIsoN’s OOD detection performance does not depend on perfectly accurate predicted classes but rather on the data characteristics.

Table 7: Classification accuracy of the primary models on ID, OOD, and combined target samples, together with CC-DIsoN OOD detection performance (AUROC from Tab. 1).

Dataset	ID Acc. (%)	OOD Acc. (%)	ID&OOD Acc. (%)	CC-DIsoN AUROC
Dermatology	77.6	54.0	63.0	89.5
Chest X-Ray	93.0	70.8	82.2	84.9
Ultrasound	78.6	61.4	64.8	65.6
MIDOG (near+far)	77.3	68.6	69.2	76.0

In Section 4.1 and Tab. 3b, we further investigate the effect of incorrect predicted classes on class-conditioning in controlled settings. Here, we describe these settings in more detail. We designed three experiment variants for Dermatology, Breast Ultrasound, and Chest X-ray by manually assigning wrong predicted classes from the primary model to specific target samples:

- All targets mislabeled (ID + OOD wrong):** All target samples, regardless of whether they are ID or OOD, are assigned a random incorrect class. This represents the extreme case of a completely inaccurate primary model (0% Accuracy), which would not be realistic in deployment but an interesting setting to obtain insights.
- Only ID targets mislabeled:** All target ID samples are assigned incorrect classes (0% Accuracy on ID), while OOD targets use their predicted classes. Again, this represents an impractical scenario for deployment, since a model with 0% ID accuracy would not be used in real-world, but useful to study misclassification behavior. Central motivation for class-conditioned sampling was to make the isolation task more difficult for ID target samples, as they should be harder to isolate from source (training ID) samples of the same class, as they share common visual features. This should lead to slower convergence and increase the difference than when separating OOD samples from source (training ID) samples, even of the same class, which is faster due to domain-shift. If we instead compare ID target samples to source (training) samples from the wrong class, the isolation will be easier, resulting in worse OOD detection.
- Only OOD targets mislabeled:** All OOD target samples are assigned incorrect classes (0% Accuracy on OOD), while ID targets use their predicted classes. This mimics a situation where domain shift causes the primary model to misclassify OOD samples, and gives us insights what would happen in the most extreme cases of domain shift. Since OOD data already differ visually from the source distribution, assigning and comparing them with unrelated classes can make their isolation even easier, and we expect an improvement in detection.

The results in Tab. 3b confirm these expectations. Performance decreases when ID targets are mislabeled, where class-conditioning is most important, while slightly increasing when OOD targets are mislabeled. Even in the extreme “all wrong” case, CC-DIsoN remains competitive and outperforms the strongest baseline (Tab. 3b) in all but one dataset. This shows that CC-DIsoN’s improvement does not rely on perfectly accurate class predictions and that the method remains robust to moderate number of misclassification errors. Overall, comparison with visually similar source samples is beneficial for DIsoN and provides stable OOD detection performance even when predicted classes are not perfect.

## F Ablation Study: Further Investigation of Image Augmentations

In Section 4.2, we showed that applying image augmentations during DIsoN training improves OOD detection across Dermatology, Chest X-ray, and Breast Ultrasound. Here, we extend this ablation study by comparing four augmentation settings: no augmentation, augmentations only on the Source Node data, only on the target sample, and on both nodes. Fig. 6 reports AUROC and FPR95 for all settings. Applying augmentations on both nodes consistently performs best. Interestingly, for Dermatology, applying augmentations only on the target sample gives best AUROC overall. We can also see that target-only augmentation outperforms source-only augmentations in most cases. One exception is Ultrasound FPR95, where source-only yields better results. These findings further strengthen our finding of the importance of regularization on especially the target sample to prevent fast memorization of superficial image-specific features, and encourage learning more meaningful features for differentiation of ID and OOD data, as discussed in Section 4.2.

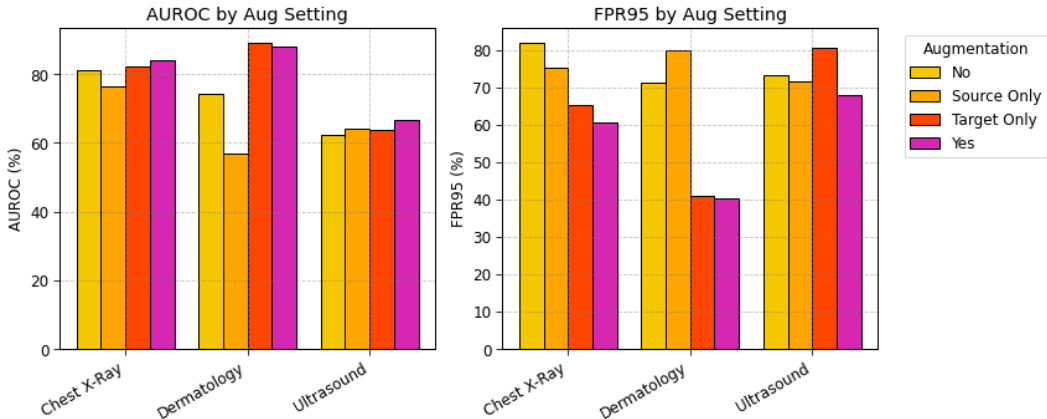


Figure 6: **Effect of applying augmentations on different nodes for DIsoN.** AUROC (left) and FPR95 (right) across three medical datasets under four augmentation settings: no augmentation, augmentations only on the source node, only on the target sample, and on both. Applying augmentations on both nodes performs best overall. Target-only augmentation outperforms source-only in most settings, highlighting the importance of regularizing the target sample during isolation.

## G Runtime Statistics

Figure 4 (a) in the main paper reports the average number of rounds required for the isolation task to converge. To provide a more detailed view of runtime variability, we report additional statistics in Table 8, including the 25th percentile, median, and 75th percentile of convergence rounds for both ID and OOD target samples using our default  $\alpha = 0.8$ . Reporting these quantiles helps practitioners assess expected runtime under different ID/OOD ratios. Since wall-clock runtime depends on hardware, we report the number of rounds as a hardware-independent measure. OOD samples generally converge in fewer rounds than ID samples, consistent with their easier separability from the source distribution.

We further analyze how the runtime distribution changes with  $\alpha$ . Tables 9-11 show that decreasing  $\alpha$  consistently reduces the number of rounds required for convergence. Importantly, OOD samples

Table 8: Quantiles (25th, median, 75th percentile) of convergence rounds for ID and OOD samples across datasets. OOD samples converge in fewer rounds and show lower variability, while ID samples display higher variability due to within-distribution complexity.

Dataset	Sample Type	25th Perc.	Median	75th Perc.
Dermatology	ID	68.0	126.5	184.0
	OOD	22.0	28.0	40.0
Ultrasound	ID	20.0	29.0	100.0
	OOD	16.0	20.5	32.0
Chest X-Ray	ID	28.0	41.0	92.0
	OOD	16.0	20.0	26.0
Histopathology (near OOD)	ID	44.3	59.5	74.0
	OOD	34.0	44.0	57.0

converge faster across all  $\alpha$ , while ID samples exhibit broader variability due to within-distribution complexity. Note that, as described above, we set the maximum number of rounds  $R_{\max}$  as the OOD score when convergence was not reached. For these additional runtime experiments, we set a lower maximum number of rounds for the Dermatology dataset from ( $R_{\max} = 300$ ) to ( $R_{\max} = 150$ ) in order to reduce computational cost. For  $\alpha = 0.90$  and  $\alpha = 0.95$ , the majority of ID samples did not converge before reaching this limit. Therefore, the 25th percentile equals  $R_{\max}$  in those cases.

Table 9: Distribution of convergence rounds (25th, median, 75th percentile) for Breast Ultrasound across  $\alpha$  values. Lower  $\alpha$  accelerates convergence, while OOD samples consistently require fewer rounds than ID samples.

$\alpha$	Sample Type	25th Perc.	Median	75th Perc.
0.95	ID	39.8	50.0	300.0
	OOD	33.0	42.0	59.0
0.90	ID	25.0	39.5	297.0
	OOD	22.0	27.0	42.0
0.50	ID	13.8	17.0	26.3
	OOD	13.0	15.0	19.0
0.40	ID	11.0	13.0	17.0
	OOD	11.0	14.0	17.0

Table 10: Distribution of convergence rounds (25th, median, 75th percentile) for Chest X-Ray across  $\alpha$  values. Lower  $\alpha$  reduces the number of rounds required for convergence, with OOD samples converging faster and more consistently than ID samples.

$\alpha$	Sample Type	25th Perc.	Median	75th Perc.
0.95	ID	51.0	58.0	75.0
	OOD	44.0	48.0	53.0
0.90	ID	26.0	35.0	100.0
	OOD	19.0	23.0	27.0
0.50	ID	20.0	27.0	51.5
	OOD	14.0	16.0	20.0
0.40	ID	15.0	17.0	23.0
	OOD	11.0	13.0	15.0

## H Practical Deployment Considerations And Runtime Comparisons

In many medical imaging workflows, real-time inference is not required. Diagnostic scans are often reviewed hours or days after acquisition due to limited clinical staff availability, and in some cases, turnaround times can extend to several weeks [31]. Within such workflows, AI models can operate asynchronously, processing scans during this waiting period. Therefore, inference times of several minutes per sample are acceptable when they provide more reliable detection of OOD samples, and similar latency is acceptable in many other non-real-time workflows outside of healthcare. DIsOn was

Table 11: Distribution of convergence rounds (25th, median, 75th percentile) for Dermatology across  $\alpha$  values. Convergence becomes substantially faster as  $\alpha$  decreases, and OOD samples consistently require fewer rounds than ID samples.

$\alpha$	Sample Type	25th Perc.	Median	75th Perc.
0.95	ID	150.0	150.0	150.0
	OOD	72.0	87.0	122.0
0.90	ID	150.0	150.0	150.0
	OOD	37.0	44.0	66.0
0.50	ID	16.0	17.0	21.0
	OOD	13.0	15.0	16.0
0.40	ID	5.0	11.0	15.0
	OOD	5.0	5.0	11.0

specifically developed for such workflows, where reliability and privacy are prioritised over speed, and these latencies remain practically acceptable. To provide a complete view of computational cost, we report both communication rounds (Appendix G) and wall-clock runtimes for comparison with other methods. Together, these results help practitioners assess whether DIsoN is suitable for their deployment setting.

DIsoN introduces additional computation at inference time (approximately 40 s–4 min per sample in our experiments on an NVIDIA RTX A5000), as each target sample requires iterative isolation training until convergence. In contrast, most compared baselines complete inference within milliseconds, since they rely on a single forward pass of a CNN backbone followed by lightweight post-processing to compute an OOD score (e.g., distance computation, linear projection, or tree traversal). Note that iForest, conceptually the closest to DIsoN, cannot be trained jointly on source and target data due to privacy constraints, unlike DIsoN. Following the original iForest formulation [25], we pre-train it only on the source (ID) data and then apply it with a single forward pass per target sample to determine whether it is ID or OOD, which explains its much lower runtime.

While this makes the baselines faster, DIsoN’s iterative optimisation results in more reliable separation between ID and OOD samples, as demonstrated in our results. Average per-sample runtimes for representative baselines on the Ultrasound dataset are reported in Table 12.

Table 12: Average inference time per target sample (seconds, NVIDIA RTX A5000). Baseline methods compute OOD scores after a single forward pass of the pre-trained network followed by lightweight post-processing, whereas CC-DIsoN performs iterative optimisation until convergence, which increases latency but yields more reliable OOD detection performance.

Method	Avg. Runtime (s)
MDS	0.006
ViM	0.005
iForest	0.015
CIDER	0.007
PALM	0.007
CC-DIsoN (ID samples)	155.2
CC-DIsoN (OOD samples)	90.9

**Single-Sample vs. Batch Processing.** DIsoN is designed to process one target sample at a time, as it learns a decision boundary that separates a single target sample from the training distribution using convergence behaviour as the OOD score. This design aligns with many real-world scenarios, especially in healthcare, where each patient scan is acquired and analysed individually rather than in large batches. If batch processing is feasible, multiple DIsoN instances can be executed in parallel to use available hardware efficiently. In our experiments, up to eight DIsoN runs could be executed concurrently on a single NVIDIA RTX A5000 (24 GB VRAM). Although not a traditional deep learning batch-tensor setup, this parallel execution allows scaling for pre-collected datasets.

**Network Conditions and Communication Latency.** DIsoN involves a single target client communicating with a source node, making it simpler and more robust than large-scale multi-client federated systems. Network delays or volatility only affect wall-clock time, not the number of communication

rounds or the quality of convergence. In practice, network disconnections can be handled through standard retry or timeout mechanisms used in distributed systems.

Overall, these experiments and considerations demonstrate that while DIsoN trades inference speed for reliability, its runtime remains predictable and manageable across deployment conditions, making it suitable for safety-critical settings where performance is prioritised and real-time inference is not required.

## I Additional Multi-Seed Results for Histopathology

Due to space limitations, Table 2 reports means over three seeds only, the standard deviations are omitted. In this section, we provide the complete tables including standard deviations. Tables 13 (AUROC  $\uparrow$ ) and 14 (FPR95  $\downarrow$ ) list the *mean  $\pm$  std* over three random seeds for the Histopathology dataset. For the Avg. columns, the  $\pm$  values are computed as the *sample standard deviation across seeds of the per-seed macro averages*.

Table 13: Complete AUROC ( $\uparrow$ ) results for the Histopathology dataset (MIDOG). Each cell shows mean  $\pm$  standard deviation over three random seeds. This extends the means reported in Table 2 with standard deviation.

Methods	near-OOD								far-OOD		
	2	3	4	5	6a	6b	7	Avg.	CCAgT	FNAC	Avg.
MSP	54.1 $\pm$ 5.8	47.4 $\pm$ 13.0	55.7 $\pm$ 2.5	59.1 $\pm$ 1.2	54.8 $\pm$ 0.6	45.6 $\pm$ 9.3	56.1 $\pm$ 5.3	53.3 $\pm$ 3.5	78.4 $\pm$ 1.4	82.7 $\pm$ 4.3	80.6 $\pm$ 1.6
MDS	67.4 $\pm$ 3.0	67.2 $\pm$ 0.6	65.7 $\pm$ 0.3	61.2 $\pm$ 4.5	60.6 $\pm$ 1.6	55.6 $\pm$ 5.9	51.0 $\pm$ 7.1	61.2 $\pm$ 1.8	87.1 $\pm$ 9.9	86.6 $\pm$ 11.9	86.8 $\pm$ 10.5
fDBD	57.9 $\pm$ 8.2	52.6 $\pm$ 8.4	57.5 $\pm$ 4.3	60.2 $\pm$ 2.4	57.9 $\pm$ 1.6	51.2 $\pm$ 6.1	55.3 $\pm$ 4.5	56.1 $\pm$ 3.8	74.6 $\pm$ 13.8	82.1 $\pm$ 0.6	78.3 $\pm$ 7.1
ViM	68.0 $\pm$ 3.6	66.7 $\pm$ 2.6	66.2 $\pm$ 1.2	63.5 $\pm$ 1.4	61.9 $\pm$ 0.9	55.7 $\pm$ 7.0	54.9 $\pm$ 5.5	62.4 $\pm$ 1.5	92.5 $\pm$ 3.4	92.6 $\pm$ 5.2	92.6 $\pm$ 4.0
iForest	37.9 $\pm$ 5.8	38.7 $\pm$ 4.8	39.7 $\pm$ 1.9	41.6 $\pm$ 6.5	39.5 $\pm$ 1.9	40.4 $\pm$ 4.3	46.4 $\pm$ 9.4	40.6 $\pm$ 1.9	27.7 $\pm$ 16.4	32.3 $\pm$ 24.3	30.0 $\pm$ 20.2
CIDER	71.4 $\pm$ 3.3	65.6 $\pm$ 8.1	55.5 $\pm$ 6.5	64.2 $\pm$ 2.5	57.4 $\pm$ 2.0	47.7 $\pm$ 10.0	64.1 $\pm$ 3.0	60.9 $\pm$ 2.2	82.5 $\pm$ 4.4	95.4 $\pm$ 3.4	89.0 $\pm$ 2.5
PALM	73.5 $\pm$ 2.3	59.2 $\pm$ 11.0	66.3 $\pm$ 5.5	64.3 $\pm$ 1.1	62.1 $\pm$ 3.9	41.8 $\pm$ 4.5	61.6 $\pm$ 2.5	61.3 $\pm$ 3.4	97.0 $\pm$ 4.0	99.6 $\pm$ 0.6	98.3 $\pm$ 2.3
CC-DIsoN	75.4 $\pm$ 1.3	79.5 $\pm$ 1.6	72.6 $\pm$ 0.6	63.0 $\pm$ 1.7	64.0 $\pm$ 2.3	70.7 $\pm$ 2.8	61.8 $\pm$ 2.0	69.6 $\pm$ 0.7	98.3 $\pm$ 0.1	98.4 $\pm$ 0.1	98.3 $\pm$ 0.1

Table 14: Complete FPR95 ( $\downarrow$ ) results for the Histopathology dataset (MIDOG). Each cell shows mean  $\pm$  standard deviation over three random seeds. This extends the means reported in Table 2 with standard deviation.

Methods	near-OOD								far-OOD		
	2	3	4	5	6a	6b	7	Avg.	CCAgT	FNAC	Avg.
MSP	94.8 $\pm$ 4.2	93.4 $\pm$ 7.0	89.4 $\pm$ 5.4	93.5 $\pm$ 0.6	94.7 $\pm$ 1.4	95.5 $\pm$ 4.4	92.4 $\pm$ 3.5	93.4 $\pm$ 1.9	52.2 $\pm$ 10.0	63.6 $\pm$ 8.4	57.9 $\pm$ 5.4
MDS	80.0 $\pm$ 3.0	79.8 $\pm$ 1.6	81.9 $\pm$ 5.0	87.4 $\pm$ 3.4	87.4 $\pm$ 2.8	89.5 $\pm$ 2.4	91.6 $\pm$ 2.9	85.4 $\pm$ 2.7	43.6 $\pm$ 20.6	39.6 $\pm$ 26.6	41.6 $\pm$ 23.1
fDBD	83.0 $\pm$ 7.2	81.4 $\pm$ 8.8	88.7 $\pm$ 2.6	89.0 $\pm$ 2.7	85.9 $\pm$ 7.9	86.2 $\pm$ 9.8	92.2 $\pm$ 1.3	86.6 $\pm$ 4.8	58.3 $\pm$ 10.8	63.7 $\pm$ 2.9	61.0 $\pm$ 6.8
ViM	79.8 $\pm$ 7.3	77.8 $\pm$ 4.3	77.7 $\pm$ 1.8	86.9 $\pm$ 3.1	87.3 $\pm$ 0.7	91.0 $\pm$ 3.4	93.1 $\pm$ 2.8	84.8 $\pm$ 2.6	29.1 $\pm$ 9.8	27.0 $\pm$ 16.2	28.0 $\pm$ 12.6
iForest	98.3 $\pm$ 2.0	96.9 $\pm$ 2.4	97.7 $\pm$ 1.8	97.5 $\pm$ 1.2	98.0 $\pm$ 1.7	97.7 $\pm$ 2.9	95.7 $\pm$ 1.2	97.4 $\pm$ 1.4	99.2 $\pm$ 0.4	96.8 $\pm$ 4.1	98.0 $\pm$ 2.1
CIDER	84.6 $\pm$ 4.7	89.0 $\pm$ 3.8	91.5 $\pm$ 1.9	89.8 $\pm$ 2.2	92.2 $\pm$ 3.0	96.5 $\pm$ 0.5	88.2 $\pm$ 5.1	90.2 $\pm$ 2.4	77.2 $\pm$ 16.5	18.3 $\pm$ 13.3	47.8 $\pm$ 6.2
PALM	78.1 $\pm$ 5.1	90.3 $\pm$ 1.8	77.7 $\pm$ 7.4	93.6 $\pm$ 0.4	90.8 $\pm$ 1.2	97.6 $\pm$ 1.4	93.6 $\pm$ 3.1	88.8 $\pm$ 0.8	21.8 $\pm$ 35.7	1.5 $\pm$ 2.5	11.6 $\pm$ 19.1
CC-DIsoN	78.8 $\pm$ 4.0	61.7 $\pm$ 3.6	79.7 $\pm$ 2.7	89.4 $\pm$ 2.4	85.3 $\pm$ 5.2	79.9 $\pm$ 5.0	92.0 $\pm$ 0.0	81.0 $\pm$ 1.2	4.8 $\pm$ 1.8	4.0 $\pm$ 1.4	4.4 $\pm$ 1.6

## J Qualitative Visualization of DIsoN Isolation Process

In this section, we provide qualitative visualizations of the DIsoN isolation process over communication rounds. Figure 7 shows PCA projections of a target sample and the source data after communication rounds 0, 15, and 25. Each row corresponds to a target image from the Dermatology dataset. In the OOD example (top row), the target sample (orange star) rapidly drifts away from the source distribution (blue points), achieving clear separation already after communication round 15. In contrast, the ID target (bottom row) remains closely clustered with the source data, showing that it is harder to isolate. This side-by-side comparison shows DIsoN’s core idea/motivation: OOD samples isolate quickly, while ID samples require more rounds.

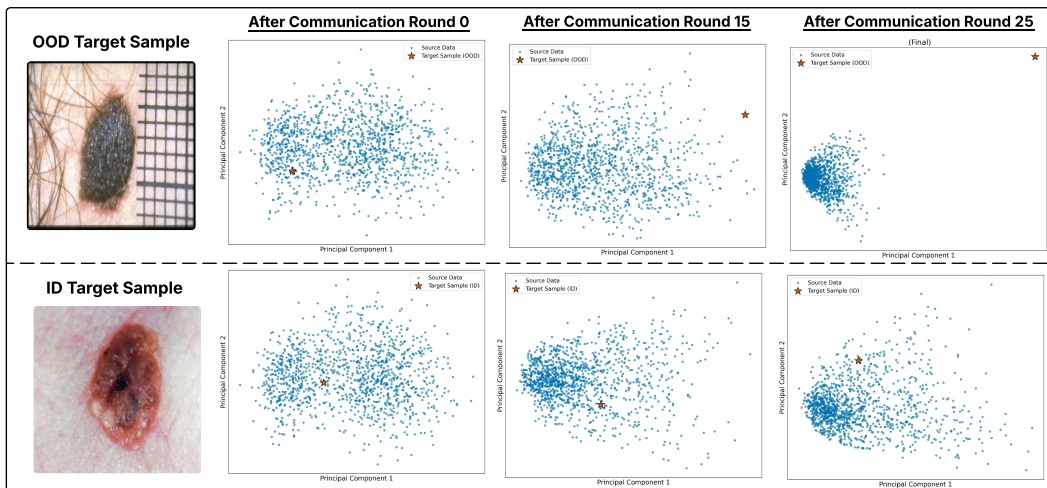


Figure 7: **Isolation Process over Communication Rounds.** PCA projections of source samples (blue) and a target sample (orange star) after communication rounds 0, 15, 25 of DIsoN training. The top row shows a target sample that is OOD, the bottom row shows a target sample that is ID (from the Dermatology dataset). The OOD sample becomes separated already after round 15 and is clearly isolated by round 25. In contrast, the ID sample remains entangled with the source distribution throughout, demonstrating that it is harder to isolate.